ChemPlusChem

Research Article
doi.org/10.1002/cplu.202300310

Chemistry Europe
European Chemical Societies Publishing

www.chempluschem.org

Four Slip-Stacked Arrangements, Three Types of Photophysics: Crystal Structure and Solid-State Fluorescence of 3,6-Diaryl Substituted Furo[3,4-*c*]furanone Polymorphs and Regioisomers

Karel Pauk,[a] Stanislav Luňák, Jr.,[b] Oldřich Machalický,[a] Franc Perdih,[c] Jan Vyňuchal,[a, d] Zdeněk Eliáš,[a, e] and Aleš Imramovský*[a]

Dedicated to Professor Miloš Nepraš in occasion of his 90th birthday.

Six symmetrical 3,6-diaryl (aryl = phenyl, 2-, 3- and 4-tolyl, 2,4- and 3,5-xylyl) substituted furo[3,4-c]furanones (DFF) were synthesized. The computational analysis, based on density functional theory, found eight possible centrosymmetrical slipped π-stack arrangements, formed according to electron repulsion minimization principle, as for previously reported for π-isoelectronic diketopyrrolopyrroles (DPP). One of these slipped stack arrangements was found to form infinite columns in the crystals of a new polymorph of parent phenyl derivative (with centre-to-centre distance CC = 6.975 Å), other three types of stacks were found for 3-tolyl (CC = 6.153 Å), 4-tolyl (CC = 3.849 Å) and 2,4-xylyl (CC = 4.856 Å) derivatives by single crystal X-ray diffractometry. All six derivatives show intense solution fluorescence in blue/green region, with a maximum driven entirely by a number and position of methyl substituents on phenyl rings. On the other hand, the solid-state fluorescence from yellow over orange to red is observed only for four derivatives and its presence/absence, spectral position and vibronic structure is driven exclusively by the slips in π-stacks (with interplanar distance always less than 3.5 Å) of almost planar DFF molecules, resulting in J-type emission, H-type excimer-like emission and H-type quenching.

Introduction

Small (non-polymeric) organic compounds with planar π-extended chromophores show semiconducting properties, comparable with the inorganic ones, in field-effect transistors (FETs).[1] High mobilities are enabled by closely packed arrangements in polycrystalline form, among which slipped face-to-face π-stacking is considered as the most efficient.[2] The electronic coupling, as a key physical attribute, driving the charge transfer, is strongly dependent on longitudinal and lateral slips of π-stacked molecules, thus the crystal engineering through polymorphism[3] or regioisomerism[4] may considerably affect the electronic properties. On the other hand, close π-stacking is usually detrimental from the point of view of the luminescence ability in solid-state, owing to the excitonic coupling,[5] resulting in a formation of H-aggregates/excimers.[6] Thus, the materials for organic light-emitting transistors (OLETs), for which both high mobility and intense luminescence is required, usually contain some degree of non-planarity and/or flexibility[7] or the rigid planar molecules are used only as the dopants in suitably

[a] *Dr. K. Pauk, Dr. O. Machalický, Dr. J. Vyňuchal, Dr. Z. Eliáš, Prof. A. Imramovský*
Department of Organic Technology
Institute of Organic Chemistry and Technology
Faculty of Chemical Technology
University of Pardubice
Studentská 95
532 10 Pardubice (Czech Republic)
E-mail: ales.imramovsky@upce.cz

[b] *Dr. S. Luňák, Jr.*
Materials Research Centre
Faculty of Chemistry
Brno University of Technology
Purkyňova 464/118
612 00 Brno (Czech Republic)

[c] *Prof. F. Perdih*
Chair of Inorganic Chemistry
Faculty of Chemistry and Chemical Technology, University of Ljubljana
Večna pot 113
1000 Ljubljana (Slovenia)

[d] *Dr. J. Vyňuchal*
Synthesia a.s.,
Semtín 103
532 17 Pardubice (Czech Republic)

[e] *Dr. Z. Eliáš*
Farmak, a.s.
Na vlčinci 16/3
Klašterní Hradisko
77900 Olomouc (Czech Republic)

Supporting information for this article is available on the WWW under https://doi.org/10.1002/cplu.202300310

arranged host-guest systems.[8] Somewhat similar design principles are also used for so called dual-state emitters.[9] Except using an above-mentioned sensitization, an increasing of structural integrity, promoting J-coupling or reducing the detrimental exciton migration to the traps are another ways to improve the intensity of solid-state fluorescence (SSF), especially in polycrystalline forms.[10] If π-stacked planar chromophores form electronically coupled isolated H-dimers in crystals, excimer fluorescence can be observed,[11,12,13] due to self-trapping. Nevertheless, it is generally difficult to realize such crystal packing in a defined way and small changes in molecular structure can switch the alternating stacking to homogenous.[12] Cyanines are probably the only class of dye chromophores, that naturally prefer the crystal packing with the "classical" J-type π-stacked columns with low slip angles.[14] The neutral molecules, in which the π-stacking is driven mainly by short-range dispersion forces, hold usually more compact arrangements with higher slip angles and thus H-type aggregation. Thus, among eight possible centrosymmetrical π-stacked arrangements in 1D infinite columns of diketopyrrolopyrroles, the only one and, furthermore, relatively less stable, should show J-type photophysics.[15] Altogether, observing intense SSF in polycrystalline materials with infinite homogenous columns, formed by H-type π-stacks, is uncommon.

Diketopyrrolopyrroles (DPPs on Figure 1, X=NH, Y=O, Ar= phenyl), like 3,6-bis-phenyl-1*H*,4*H*-pyrrolo[3,4-*c*]pyrrole-1,4-dione (Pigment Red–P.R. 255, or its 4,4'-dichloro derivative, Pigment Red-P.R. 254), are organic pigments,[16] with almost planar molecules fixed in crystals by in-layer CO–HN hydrogen bonding and inter-layer face-to-face slipped π-stacking for both pigments and, furthermore, by halogen-π edge-to-face interaction in P.R. 254.[17] If at least partially soluble, PhDPP (Ar= phenyl) pigments intensely fluoresce in solution.[18] *N*,*N*'-dialkylation of DPP core disables this type of hydrogen bonding and brings considerable differences between planarity and (consequent) ability of close π-stacking for PhDPP and ThDPP (Ar= thiophen-2yl) derivatives. If R=*n*-hexyl, diphenyl derivative becomes non-planar, π-stacking is weak and moderate SSF is observed, while dithiophenyl derivative remains planar, closely π-stacked with very weak SSF, as the dominant excited state deactivation is nonradiative, generating triplet states through singlet fission.[19] An absence of SSF in closely packed PhDPP pigments with various substituted phenyls and its presence after alkylation is quite a common process[20] and all DPPs intensely fluorescent in solid-state are the *N*,*N*'-dialkylated derivatives with PhDPP core.[21] On the other hand, DPP pigments irrespective to Ar show moderate mobilities in FETs,[22] just as *N*,*N*'-dialkylated ThDPPs.[23] The latter ones are also efficient in organic photovoltaics,[24] due to their ability to transfer both charge and exciton.

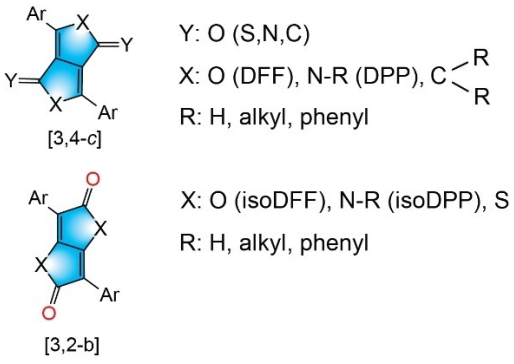

Figure 1. General formula of the diones of fused five-membered rings.

Above mentioned diketopyrrolopyrroles are a special subclass of the symmetrical diones (Y=O) of two fused 5-membered rings, connected in [3,4-c] manner (Figure 1). Their positional isomers with the rings connected by [3,2-b] type fusion are called iDPPs[25] or isoDPPs[26]. Parent isoDPP (Ar = phenyl, X=NH), just as its π-isoelectronic analogue, i.e. the lichen compound pulvinic dilactone (X=O)[27], does not fluoresce even in solution, due to the low-lying symmetry-forbidden ππ* state.[25] The same reason probably causes very weak solution fluorescence of thieno[3,2-*b*]thiophene 2,5-diones (Ar=Th, X=S).[28] [3,4-c] fused compounds have bright lowest excited state and thus generally fluorescence in solution as shown for planar parent PhDPP (X=NH) and PhDFF (X=O)[25] and also for non-planar pentalenediones ($X=C(CH_3)_2$)[29]. The latter compounds show also SSF[29], so as the non-planar *N*,*N*'-alkylated PhDPPs. The solution fluorescence of [3,4-c] fused compounds can be considered as general and is quenched only by a heterosubstitution transforming them to thioketones (Y=S),[22b] because of the nπ* character of the lowest excited state, and PP-cyanines (Y=C)[30] or -azacyanines (Y=N).[31] While the presence/absence of the fluorescence in solution and in solid-state of the known subclasses of compounds from Figure 1 can be rationalized and related to the molecular structure, especially to its ability to avoid close π-stacking through molecular non-planarity, an ability of planar PhDFFs to show SSF is a bit confusing. Although both phenyl[32] and 2-tolyl DFFs[33] (compounds **3a** and **3b** on Scheme 1) are almost planar according to X-ray diffractometry (XRD), both fluoresce in solution, but SSF is reported only for the former one[33]. Such discrepancy provoked us to study this a bit overlooked class of compounds in deep. Our first experiments on **3a** were quite surprising: 1) we found out that SSF maximum of our derivative was bathochromically shifted compared the reported one[33], and 2) we consequently found, that another polymorph, than the reported one[32], was prepared. We found four types of specific intermolecular interactions in a new polymorph: slipped π-stacking with longitudinal and lateral slips only once before observed among DPPs,[15,19] CO–O interaction, CO–HC type „hydrogen bonding", involving *meta* hydrogen, and T-shaped edge-to-face CH-π interaction, involving *para* hydrogen. Consequently, we synthesized a series of symmetrical dimethyl and tetramethyl derivatives (Scheme 1), where the methyl substituents were supposed to switch off at least one of the latter two intermolecular interactions with hydrogen participation in **3a** polymorph and thus change the packing in crystal, without significant affecting molecular planarity. As we will show, the dramatic differences in the presence/absence, colour and vibronic structure of SSF were observed and the solid-state photophysics was interpreted

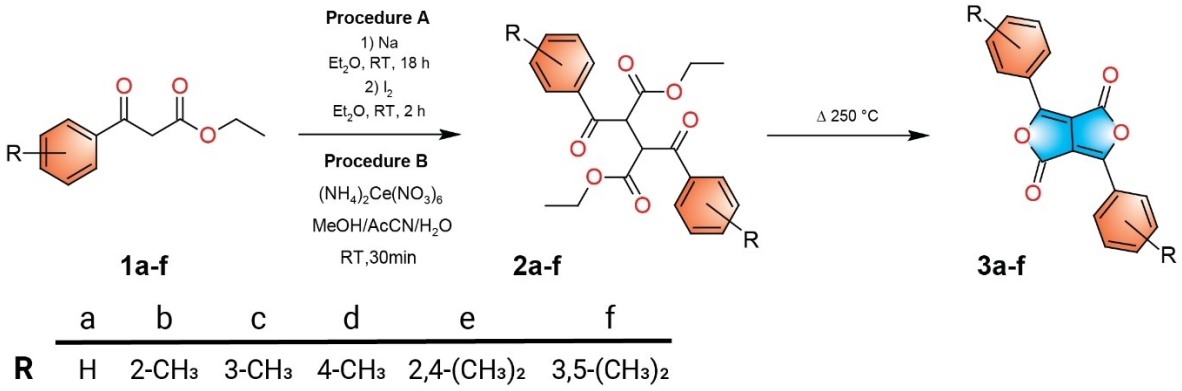

Scheme 1. Syntheses of the compounds under study.

as driven exclusively by crystal arrangement, induced by molecular regioisomerism.

Results and Discussion

3,6-Diaryl substituted furo[3,4-*c*]furanones **3a**–**f** were prepared in three steps from commercially available acetophenones according to Scheme 1. Acetophenones were converted in to the corresponding ethyl 3-oxo-3-phenylpropanoates **1a**–**f** by reaction with diethyl carbonate and sodium hydride in high yields, which corresponds to the literature.[34] Dimerization of the ethyl 3-oxo-3-phenylpropanoates **1a**–**f** was carried out in two ways: by oxidation with sodium[35] or oxidation with ceric ammonium nitrate.[36] Both of these methods gave similar yields that were mainly dependent on the methyl position on the benzene ring in the range 13–60%. However, it was found that two *meso* forms of diethyl 2,3-dibenzoylsuccinates and also by-product diethyl 2,3-dibenzoyl fumarate were formed during the reaction. Undesirable diethyl 2,3-dibenzoyl fumarate not only prevents the formation of the final 3,6-diaryl substituted furo[3,4-*c*]furanones **3a**–**f**, as it crystallizes in mixtures together with *meso* forms, but also negatively affects the crystallization of the final products, i.e. an eliminating even the traces of the impurities in the intermediates **2a**–**f** before final ring closure is decisive for the crystal growth of the final products **3a**–**f**. This unwanted by-product can be removed by suitable multiple crystallization from cold ethanol and then from EtOAc. By our empirical experience, the oxidative dimerization according to procedure B, using ceric ammonium nitrate as an oxidative agent, required usually a lower number of purifying crystallization steps. The final ring closure to 3,6-diaryl substituted furo[3,4-*c*]furanones **3a**–**f** was performed by a solvent-free thermal reaction at 250 °C under high vacuum,[33] which is the very first described procedure for four derivatives of 3,6-diaryl substituted furo[3,4-*c*]furanones **3c**–**f**. This procedure offer three brand-new **3c**, **3e** and **3f** and three **3a**, **3b** and **3d** literature-known 3,6-diaryl substituted furo[3,4-*c*]furanones.

Single crystals of **3a**, **3c** and **3e** were prepared by crystallization from toluene. Each derivative was introduced into a 5 ml flask and dissolved in toluene under heat. A saturated solution was placed into a preheated oven (110 °C), where a decreasing temperature gradient of 0.24 °C/h was set and after 15 days the resulting monocrystal was prepared. Monocrystal of **3d** was prepared by sublimation at 130 °C, pressure 10^{-3} Pa for 48 h. A distinct similarity between the measured powder XRD and the one computed from single crystal XRD (file TEYBEE from CCDC) confirmed, that **3b**, synthesized in this work, has the same crystal structure as previously reported.[33] Full crystallographic information from XRD on **3a**, **3c**, **3d** and **3e** is summarized in Table S1 in SI. Here we point out only the structural features closely related to the absorption and fluorescence in solution a SSF, i.e. molecular planarity and conformation, specific interactions, decisive for crystal packing, and nearest-neighbour distances and orientation, relating to excitonic coupling and consequently to general photophysical behaviour.

Molecules in a crystal of a new polymorph of **3a** are centrosymmetrical, nearly planar with phenyl torsion 3.9^0 as for original polymorph (3.4^0, from file BZSCLC from CCDC [32]). There were found four types of nearest-neighbour (NN) arrangements with centre-to-centre (CC) distances between 5.5 Å and 9.5 Å (Figure 2). Molecules form π-stacked columns based on centrosymmetrical dimers with a pairwise overlap between phenyl and one of the furanone rings of adjacent molecule (Figure 2a), on the contrary to the original polymorph, in which only an overlap between phenyls, each coming from a different molecule, is observed. Plane-to-plane distance (PP) between coplanar furofuranone cores is quite low (PP = 3.176 Å, Figure 2a). Molecules in layers are pairwise connected by CO–HC "hydrogen bonds", involving *meta* phenyl hydrogens (Figure 2b). Such a type of intermolecular interaction is also found in an original polymorph, but forming a four-membered macrocycles, i.e. not pairwise arranged. Low slip angle of the π-stacks is ensured by four identical CH-π interactions per each molecules (Figure 2c), in which each phenyl is both a donor of *para* hydrogen and π-acceptor. This interaction is missing in the original polymorph. On the contrary, pairwise inter-layer and inter-columnar packing motif, based on CO–O interaction (Figure 2d), is almost identical in both polymorphs (with CC = 5.777 Å for the original and CC = 5.640 Å for the new polymorph). We note only, that we were unable to find such

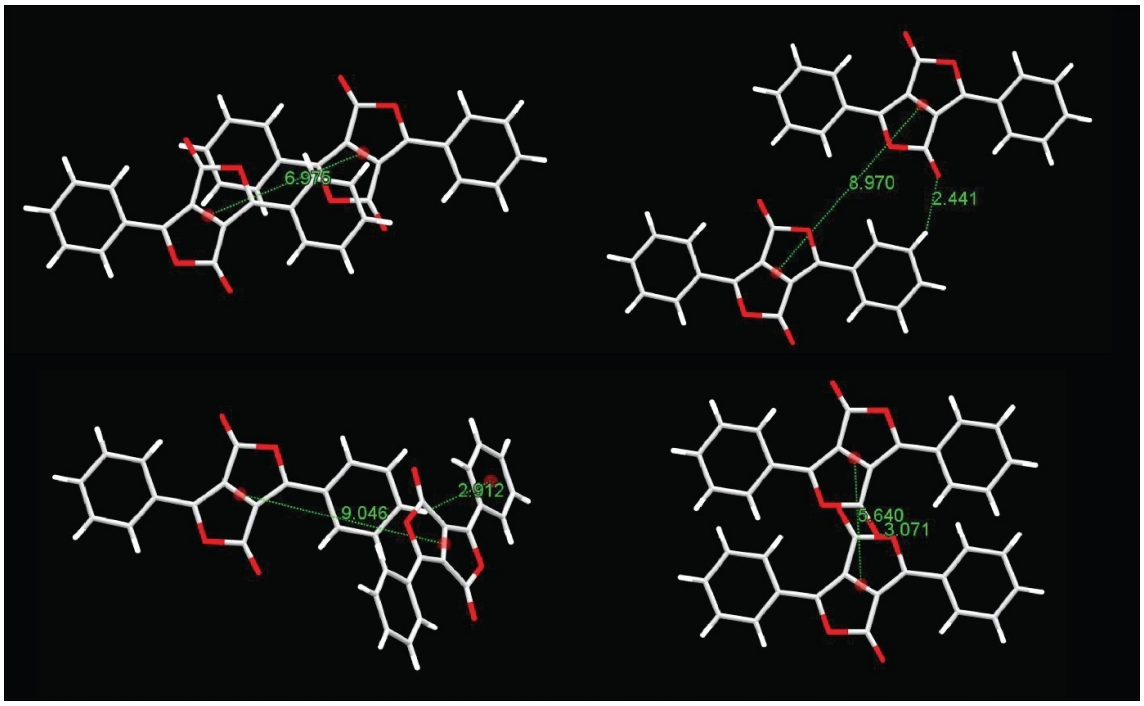

Figure 2. Nearest-neighbour interactions in a crystal of a new polymorph of **3a**. a) Left-up: in-column π-stacked dimer (CC = 6.975 Å, PP = 3.176 Å), b) right-up: in-layer CO-HC bonded (2.441 Å) dimer with CC = 8.970 Å, c) left-down: CH-π (2.912 Å) bonded dimer with CC = 9.046 Å, d) right-down: inter-column/inter-layer CO–O (3.071 Å) bonded dimer with CC = 5.640 Å.

crystallization conditions, which would lead to the formation of the original polymorph.

Both **3b** (file TEYBEE from CCDC[33]) and **3e** form the same (more stable and more planar) rotamer with *ortho* methyls closer to –O– than to O(=C) atom as shown on Figure 3. 2-Tolyl and 2,4-xylyl rings show a bit higher torsion (6.3° and 8.3°, respectively) than the phenyl one. Both **3b** and **3e** show compact columnar π-stacks (Figure 3), in which each tolyl/xylyl ring partially overlaps both furanone rings of adjacent molecule, characterized by CC distances 4.833 Å and 4.856 Å, respectively, and PP distances 3.422 Å and 3.489 Å, respectively. All other NNs have CC distance higher than 9 Å for both compounds. Except the π-stacks, other specific interactions, observed for **3a**, are limited: distinct CH- π and CO–O interactions are missing, while CO-HC one is present (involving *meta* phenyl hydrogen, lying between both methyls in **3e** case), but it is not pairwise and not in-layer.

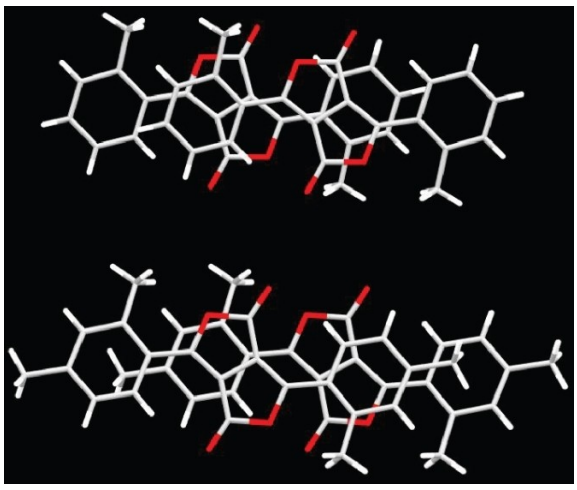

Figure 3. In-column π-stacked dimers of **3b** (up, extracted from file TEYBEE[33]) and **3e** (down).

Compound **3c** forms the columns with relatively high CC = 6.153 Å and low PP = 3. 332 Å (Figure 4) and the most planar molecular structure with 3-tolyl twist only 2.1°. As in **3b**, each tolyl ring partially overlaps both furanone rings of adjacent molecule. The second NN (CC = 7.905 Å) comes from adjacent column fixed by CO-HC interaction with *ortho* phenyl hydrogen (2.545 Å) and with methyl hydrogen. 4-Tolyl torsion angle (3.9°) in a molecule of **3d** is also relatively low. Molecules form columns with the most compact π-stacks in a series (Figure 4), in which two pairwise separated overlaps are present – between adjacent phenyls and between adjacent furofuranones, characterized by CC = 3.849 Å and PP = 3.343 Å. All other NNs have CC distance higher than 10 Å. The specific interactions, like CH– π and CO–O, are not present. CO group does not interact with phenyl hydrogens, but only with the methyl ones. We note only that **3d** formed twinned structure. Computational solution presented here gives realistic torsion angles and intermolecular distance, but some valence angles are a bit deformed.

Quantum chemical calculations found the same set of eight possible centrosymmetrical slipped π-stacks of **3a** (Figure 5) as for PhDPP.[15] Geometrical characteristics and binding energies are summarized in Table 1. All dimer geometries on Figure 5 and in Table 1 come from central dimers extracted from

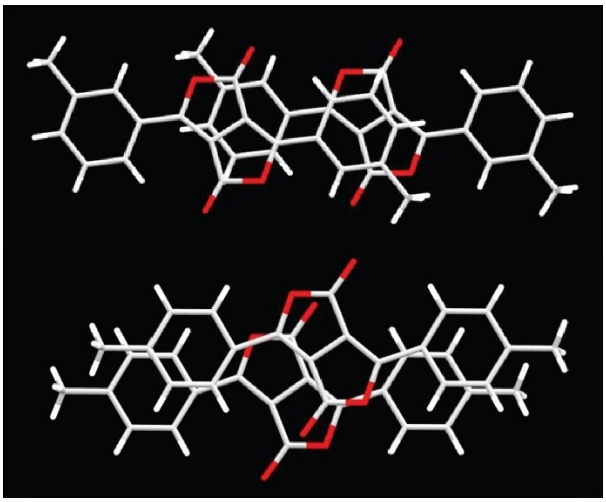

Figure 4. In-column π-stacked dimers of 3c (up) and 3d (down).

optimized 3x2 hexamers, in which three molecules in each layer (Figure S1) were fixed by C═O attraction to phenyl hydrogens either in positions 2 and 3 (dimers **1**–**7**) or 3 and 4 (dimer **8**), formally substituting the natural CO–NH in-layer hydrogen bonds used for modelling of DPP pigments.[15] Only dimers **1**–**5** could be obtained by dimer optimization of **3a**, while for *meta* tetramethylated **3f** (and for the less probable rotamer, than observed in crystal of **3c**) also a minimum, relating to dimer **6**, was computed.

Four of these eight model π-stacks were found experimentally to form the infinite columns in crystals of **3d** (dimer **1**, Figure 4), **3b** and **3e** (dimer **3**, Figure 3), **3c** (dimer **5**, Figure 4) and **3a** (dimer **6**, Figure 2a). Lower binding energy of dimer **6**, compared to the dimers **1**, **3** and **5** (Table 1), and its inability to form a self-standing minimum in a dimer approximation explain, that's why this π-stack arrangement needs a significant support of further specific interactions (CO-HC, CH-π and CO–O) to be stabilized, i.e. to avoid a slip to the more stable arrangement. In fact, this is only the second report on a detection of this rare type of packing within DFF/DPP family[15,19]. On the other hand, stacking in dimer **1**, **3** or **5** fashion is quite common between DPPs, e.g for P.R. 255[17a], its thioketo heteroanalogue[22b] and *N*,*N*′-diethyladamantanyl ThDPP[23c], respectively.

Another evidence of π-stacking arrangements driven by an electron repulsion minimization principle and the role of specific intermolecular interactions in stabilizing π-stacks with lower binding energy comes from a positional isomer of **3a**, i.e. pulvinic dilactone. Computational analyses found eight possible arrangements as for **3a** (Table 2, Figure 6). Experimental structure confirms its planarity (phenyl torsion 2.2°) and relates to π-stacking in dimer **7** fashion (Figure 7a), i.e. with relatively low binding energy (Table 2). And this weak π-stacking is fixed by the same set of further supporting interactions (CO–HC, CH-π and CO–O, Figure 7b**cd**) as for **3a** (Figure 2b**cd**). We note only, that, as for DPPs,[15] an electron repulsion minimization is manifested by a tendency of one of six negatively charged

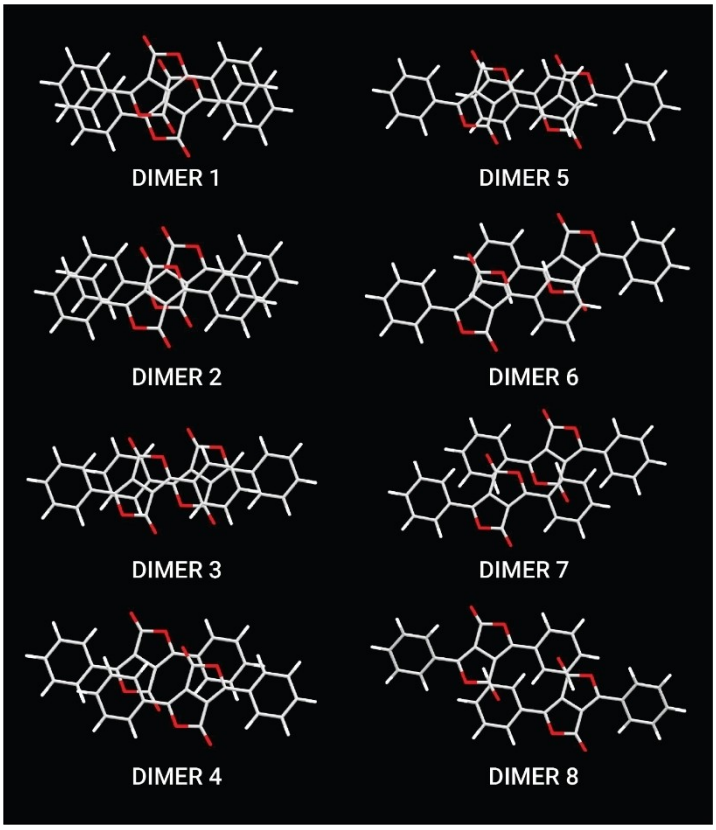

Figure 5. Front view on the computed arrangements of dimers **1**–**8** of compound **3a** from Table 1. O = red, H = white, C = grey.

Table 1. Computed centre-to-centre (CC) and plane-to-plane (PP) distances [Å], and binding energies E_{bind} [kcal/mol] of eight model dimers of **3a** on Figure 5. Binding energies were computed at M06-2X/6-311+G(2d,p) level with involved counterpoise procedure. Geometries of the dimers **1**–**7** were extracted from 3x2 hexamer type 23 (Figure S1 for dimer **3**), optimized at M06-2X/6-311G(d,p) level. Dimer **8** was extracted from 3x2 hexamer of type 34 (Figure S1 for dimer **3**), optimized also at M06-2X/6-311G(d,p) level.

Dimer	CC	PP	E_{bind}
1	3.483	3.057	13.14
2	3.528	3.066	12.87
3	4.806	3.184	14.14
4	4.729	3.028	11.18
5	6.169	3.276	12.49
6	6.561	3.125	7.57
7	5.434	3.009	8.33
8	6.802	2.901	1.38

Table 2. Computed centre-to-centre (CC) and plane-to-plane (PP) distances [Å], and binding energies E_{bind} [kcal/mol] of eight model dimers of pulvinic dilactone on Figure 6. Binding energies were computed at M06-2X/6-311+G(2d,p) level with involved counterpoise procedure. Geometries of the dimers **1**–**2** were extracted from 3x2 hexamer type 23 (Figure S2 for dimer **7**) optimized at M06-2X/6-311G(d,p) level. Dimers **3**–**8** were extracted from 3x2 hexamer of type 34 optimized also at M06-2X/6-311G(d,p) level. Dimers **6** and **8** were extracted from 3x2 hexamers of a *meta* chloro derivative of pulvinic dilactone, optimized at the same level and chlorines were then exchanged to hydrogens with C–H distance taken from monomer optimization (1.08 Å).

Dimer	CC	PP	E_{bind}
1	3.692	3.071	13.43
2	3.638	3.029	12.74
3	4.613	3.103	14.64
4	5.069	3.114	12.58
5	6.290	3.345	12.62
6	6.459	2.666	6.18
7	5.144	2.698	8.36
8	7.220	3.017	6.00

atoms of DFF or isoDFF core, identified by Mulliken charges (Figure 8), to adopt a position near the center of a phenyl ring od adjacent molecule in stack. While the dimers **4**, **6**–**8**, with the geometry driven by one of four oxygen atoms, can be found in both sets (Figures 5 and 6), there are the differences between DFF and isoDFF arrangements of dimers **3** and **5**. In both cases the negatively charged carbon atom is bonded to carbonyl carbon, but in the case of DFF negatively charged carbons belong to the central C–C bond, while in isoDFF these are the phenyl substituted carbons of a core (Figure 8). This difference is better seen on more stable dimer **3**, than on dimer **5**, as an overall geometry of pulvinic dilactone disables to adopt and ideal mutual position in this type of a stack. Furthermore, the carbon atoms in isoDFF carry the lowest negative charge (−0.16), thus their driving force for a repulsion minimization is the lowest among all relevant atoms.

Partially summarizing: 1) any symmetrical dimethylation of **3a**, leading to one of the regioisomers **3b**–**3d**, avoids some of the supporting interactions in crystal of **3a** and causes a slip of a less stable π-stacked arrangement to some of the self-standing ones, depending on methyl positions and 2) ortho dimethylated compounds **3b** and **3e** show a bit higher torsion angles ($\varphi > 6°$) and, consequently, bigger interplanar distances (PP > 3.42 Å), while *meta* and *para* regioisomers are more planar ($\varphi < 4°$) with, consequently, closer π-stacking (PP < 3.35 Å).

Absorption and fluorescence spectra and photoluminescence quantum yields (PLQY) were measured in dichloromethane (DCM). The results are shown on Figure 9 and summarized in Table 3. As PLQY is always higher than 50%, the fluorescence is dominant excited state deactivation channel for all six derivatives in solution. The absorption spectra of parent **3a** and compounds **3c**, **3d** and **3f**, methylated only in *meta* and *para* positions, show well resolved vibronic progressions with 0–0 maxima. On the other hand, compounds with *ortho* methyls (**3b** and **3e**) show blurred vibronic structure with the 0–1 maximum. Model DFT calculations found two symmetrical rotamers of **3b** with torsion angles 0^0 (the most stable one, found experimentally, Figure 3) and 39^0 (1.94 kcal/mol less stable one) and one asymmetrical (with torsion angles 4^0 and 40^0 and 1.11 kcal/mol higher energy). Thus, we consider the absorption spectrum of **3b** (and also **3e**) as an envelope of the absorptions of these three planar/nonplanar rotamers. Raising rigidity with respect to aryl torsion in the emitting state causes well resolved fluorescence spectra with 0–0 maxima in all cases. Fluorescence excitation spectra do not deviate from the absorption ones significantly. An ordering of the experimental fluorescence maxima agrees with the computed ones (Table S2), thus we consider the shoulders on short-wavelength part of the spectra of **3b** and **3e** (at about 460 and 470 nm, respectively) as a manifestation of an asymmetrical rotamers and not as a suppressed 0–0 transition. *Ortho* (**3b**), *meta* (**3c**) and *para* (**3d**) methyl substituents bring about the shifts 18 nm, 4 nm and 11 nm, respectively, in fluorescence 0–0 maxima with respect to parent **3a**. The effect of the second methylation is additive (30 nm for 2,4- xylyl **3e** and 8 nm for 3,5-xylyl **3f**), thus we can conclude, that the bathochromic shifts of the fluorescence maxima in solution are given exclusively by an

Table 3. Absorption (λ_A) and fluorescence emission (λ_E) maxima, molar absorption coefficients (ε_A) in maximum (λ_A), and fluorescence quantum yields (PLQY) in DCM. Fluorescence excitation (λ_{Ex}) and emission (λ_{Em}) maxima in solid state.

Compound	DCM solutions				Solid state	
	λ_A [nm]	ε_A [mol/L/cm]	λ_E [nm]	PLQY	λ_{Ex} [nm]	λ_{Em} [nm]
3a	455	43400	463	0,85±0,06	506	548
3b	440	47300	481	0,55±0,04	–	–
3c	459	47800	467	0,70±0,05	520	588
3d	466	57300	474	0,87±0,07	520	620
3e	450	32400	493	0,85±0,06	–	–
3f	462	49300	471	0,92±0,07	514	589

Research Article
doi.org/10.1002/cplu.202300310
Chemistry Europe
European Chemical Societies Publishing

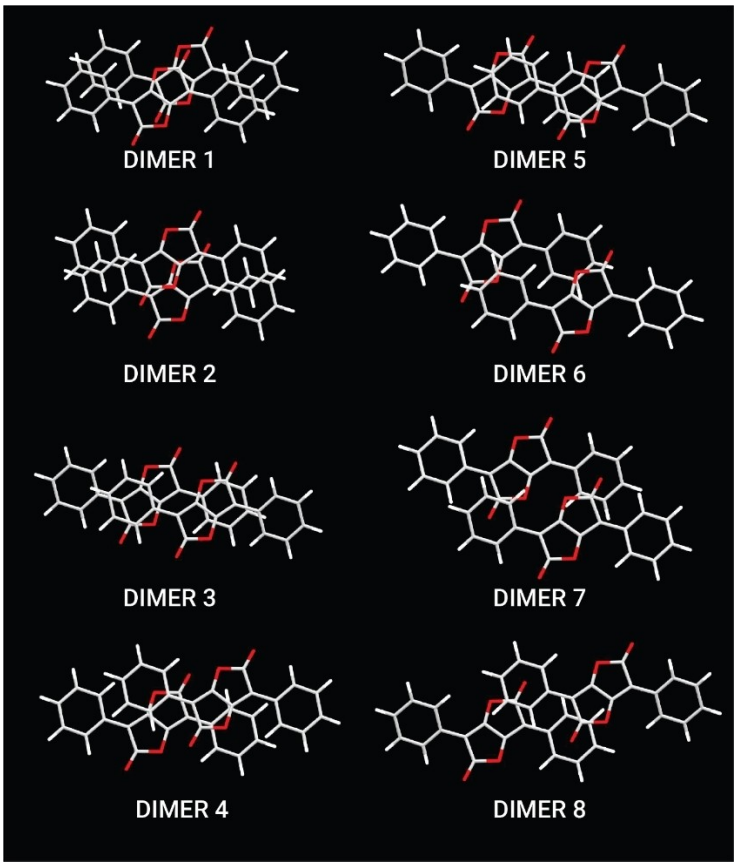

Figure 6. Front view on the computed arrangements of dimers **1**–**8** of pulvinic dilactone from Table 2. O = red, H = white, C = grey.

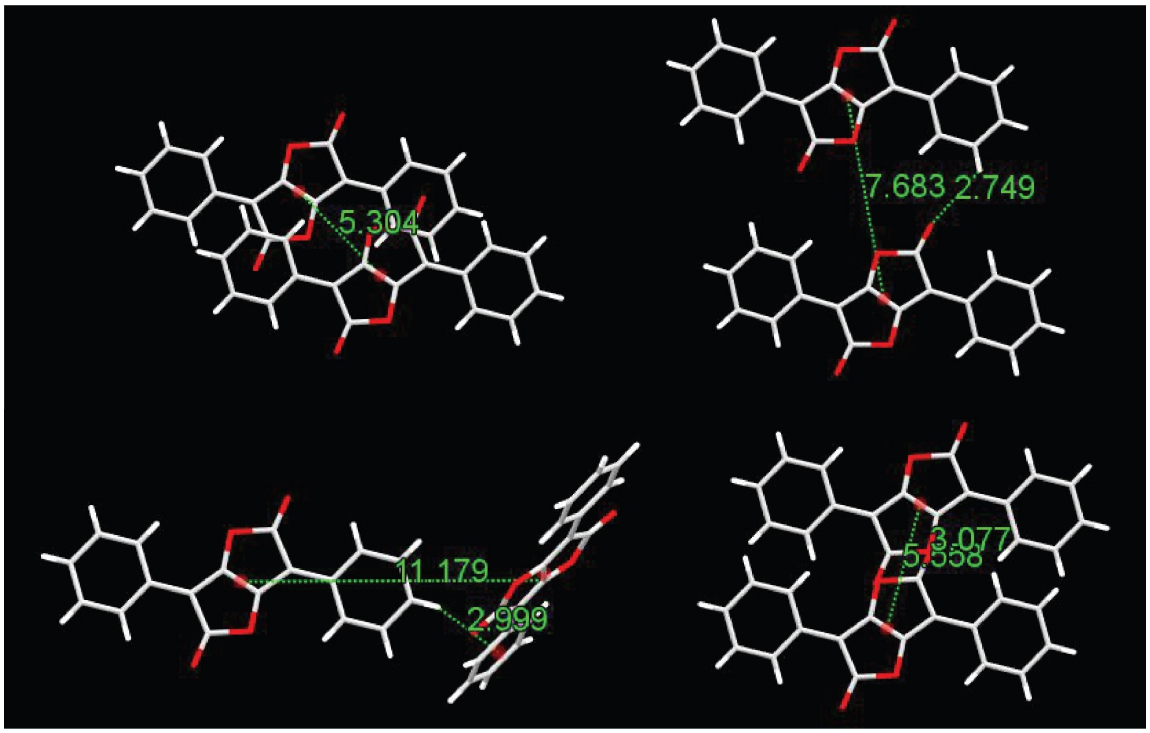

Figure 7. Nearest-neighbour interactions in a crystal of pulvinic dilactone (extracted from file ERIVEJ [27]). a) Left-up: in-column π-stacked dimer (CC = 5.304 Å, PP = 3.192 Å), b) right-up: in-layer CO-HC bonded (2.749 Å) dimer with CC = 7.683 Å, c) left-down: CH-π (2.999 Å) bonded dimer with CC = 11.179 Å, d) right-down: inter-column/inter-layer CO–O (3.077 Å) bonded dimer with CC = 5.558 Å.

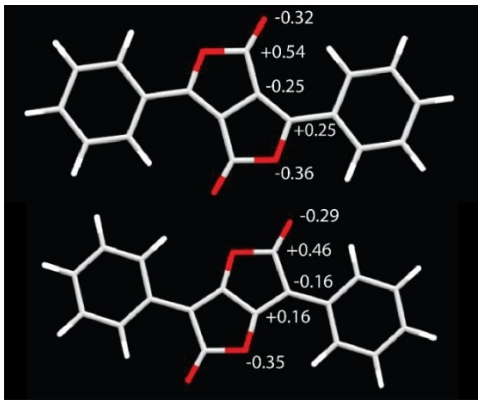

Figure 8. Mulliken charges on the atoms of central cores of **3a** and pulvinic dilactone.

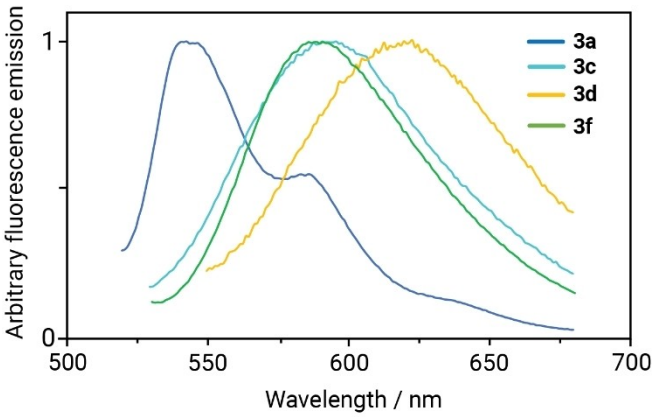

Figure 10. Fluorescence emission spectra of **3a** (blue), **3c** (cyan), **3d** (orange) and **3f** (green) in solid state.

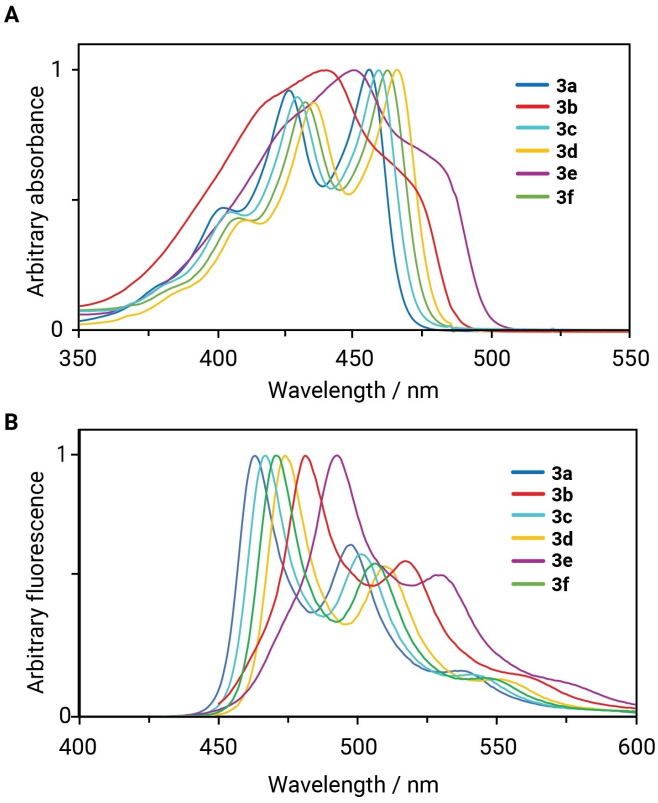

Figure 9. The absorption (**A**) and fluorescence emission (**B**) spectra in DCM for **3a** (blue), **3b** (red), **3c** (cyan), **3d** (orange), **3e** (magenta) and **3f** (green).

electronic effect (hyperconjugation) of methyl substituents. The Stokes shift is very small (~400 cm^{-1}) for planar derivatives (**3a**, **3c**, **3d** and **3f**) and considerably higher (~1.940 cm^{-1}) for the non-planar ones (**4b** and **4e**).

Only four of six derivatives show solid-state emission under UV illumination, detectable by naked eye (Figures 10 and 11, Table 3). Generally, three types of behaviour after excitation of solid powders were observed: 1) SSF with marginal intensity for compounds **3b** and **3e**, 2) yellow SSF with 0–0 maximum and the lowest DCM-to-solid shift (85 nm, 0.415 eV) and the lowest Stokes shift 42 nm (0.188 eV) for compound **3a** and 3) orange to red SSF with unresolved vibronic structure and bigger DCM-to-solid shift 118 nm (0.528 eV), 121 nm (0.546 eV) and even 146 nm (0.616 eV) for **3c**, **3f** and **3d**, respectively. It is clear, that the presence or absence of SSF, its spectral position and vibronic structure does not follow the behaviour in solution and is driven exclusively by solid-state packing. Although all five compounds from the set with known crystal structure (**3a**–**3e**) show π-stacking with PP < 3.5 Å, a bit surprisingly only two of them (**3b** and **3e**) show aggregation caused quenching (ACQ).

Compound **3a** with dimer **6** type π-stacking is the only one with expected J-type photophysics (Table 4), due to the negative excitonic coupling and thus bright lowest excited state.[37] Although this dimer is only the second nearest according to CC distances (Figure 2a**d**), which disables undoubted estimation of prevailing of J- or H-type aggregation from the crystal structure,[38] TD DFT computations (Table S4, Figure S5) show, that dimer **6** truly represents the bottom of an excitonic band, as an absolute energy of the dimer with lowest CC in **3a** crystal (Figure 2d) lies more than 0.06 eV above the energy of the lowest bright state of dimer **6**. Consequently,

Table 4. Energy of monomer-to-dimer shift $E_{DM} = E_{exc}$(monomer, $1A_u$) – E_{exc}(dimer, $1A_u$), excitonic coupling $E_{EC} = {}^1/_2$ (E_{exc}(dimer, $1A_u$) – E_{exc}(dimer, $1A_g$)), energy splitting between allowed CT and FR state $E_{CF} = E_{exc}$(dimer, $2A_u$) – E_{exc}(dimer, $1A_u$) and the ratio of their intensities $R_{FC} = f_{osc}$(dimer, $1A_u$)/ f_{osc}(dimer, $2A_u$), computed on model dimers of 3a from Tab. 1. Negative value of E_{EC} corresponds to *J*-aggregate, positive value corresponds to *H*-aggregate. E_{exc} and f_{osc} were taken from Tab. S3 with ωB97X-D/6-311+G(2d,p) excitation energies.

Dimer	E_{DM} [eV]	$2.E_{EC}$ [eV]	E_{CF} [eV]	R_{FC}
1	−0.083	+0.393	0.084	2.18
2	+0.122	+0.133	0.498	1.67
3	+0.097	+0.089	0.546	5.34
4	−0.056	+0.307	0.297	16.87
5	+0.102	+0.093	0.719	14.25
6	+0.094	−0.046	0.823	213.00
7	+0.059	+0.035	0.664	168.38
8	−0.076	+0.213	0.762	184.57

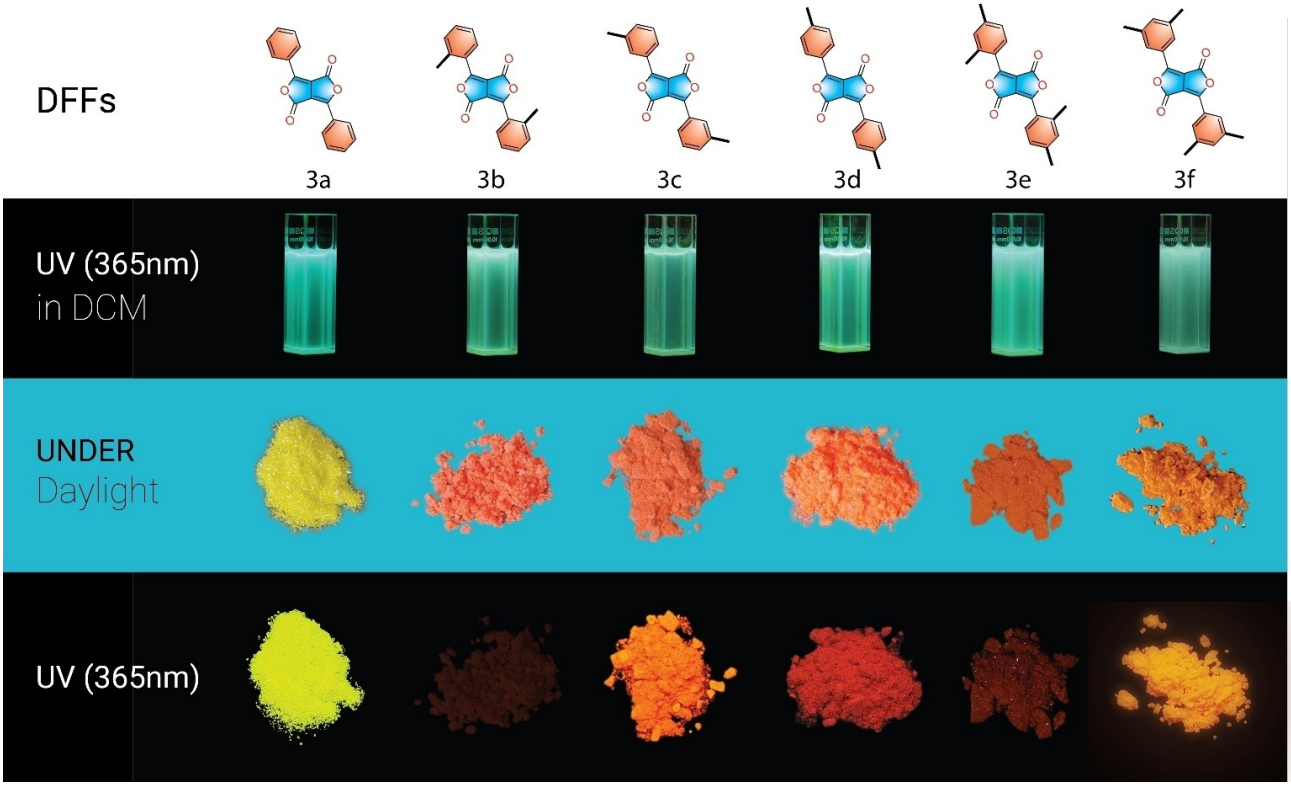

Figure 11. The photos of **3a**–**3f** in solution and in powder form under daylight and UV illumination.

yellow SSF of **3a** with 0–0 maximum is ascribed to J-type emission. The ratio of 0–0 intensity with respect to 0–1 intensity is not higher, than in solution, as expected for J-aggregates[5]. This can be explained by a coincidence of several factors: the experimental intensity of 0–0 band may be partially decreased by a reabsorption in powder samples, final spectrum is a resultant of opposite J/H type couplings of various NN pairs (Figure 2) and negative excitonic coupling in dimer **6** is quite low (Table 4). While the previously reported absorption and fluorescence maxima of **3a** in chloroform are the same or only 2 nm shifted with respect to DCM,[33] SSF maximum of a new polymorph is 20 nm red shifted as a result of more efficient J-type π-stacking.

Four methylated derivatives **3b** - **3e** form clear H-aggregates, as π-stacked dimers **1**, **3** and **5** represent strongly electronically coupled nearest neighbours in crystals. Thus the question is, why e.g. regioisomeric compounds **3b** and **3c**, forming dimers **3** and **5** with relatively similar excitonic coupling (Table 4), show ACQ and orange SSF (Figure 11), respectively. The shape and bathochromic shift of SSF spectra of **3c**, **3d** and **3f** is typical for conventional excimer-type emission[39]. Generally, an exciton transfer along π-stacked columns to the dark traps either in volume or on surface, i.e. trap-controlled emission quenching, is a common non-radiative deactivation process for polycrystallines.[10] Formation of the excimers, i.e. electronically coupled H-type dimers with partial charge-transfer (CT) character of an excitation and strong coupling between electrons and intermolecular phonons, can be considered as a self-trapping process with respect to exciton migration. We see two reasons, why compounds **3c**, **3d** and **3f** form the bright excimers, while compounds **3b** and **3e** do not. First, at least **3c** and **3d** form remarkably tighter π-stacks, increasing thus a chance for a creation of an excimer by a motion along some suitable intermolecular coordinate[39]. Second, if characterizing the lowest forbidden excited state of the dimers **1** (**3d**) and **5** (**3c**) by natural transition orbitals (NTOs), we see (Figure 12) very similar character of both transitions. "Hole" is localized on each molecule of a dimer, while "particle" is partially delocalized in a space between both monomers. Such a redistribution of an electron density is a) a signature of a partial CT character of a transition and b) an electron density between the monomers can efficiently couple with intermolecular phonons, manifested by blurred vibronic structure of SSF. On the other hand, no significant increase of an electron density, when going from "hole" to "particle" (Figure 12), is observed for dimer **3** (**3b**). As the SSF of compound **3f** is very similar to that of **3c** (Figure 10), we suppose the similar packing of these only in *meta* positions methylated derivatives. As the SSF of compound **3e** is missing so as for **3b** (Figure 11), and as they both pack in dimer **3** fashion, we suppose the similar nonradiative deactivation mechanism for both *ortho* methylated derivatives.

Although an investigating of the excited state either translational or rotational motion leading to excimer formation[40] is out of the scope of this research, we have to point out the striking difference between the presence and absence of excimer emission for **3d** and PhDPP (P.R. 255), respectively.

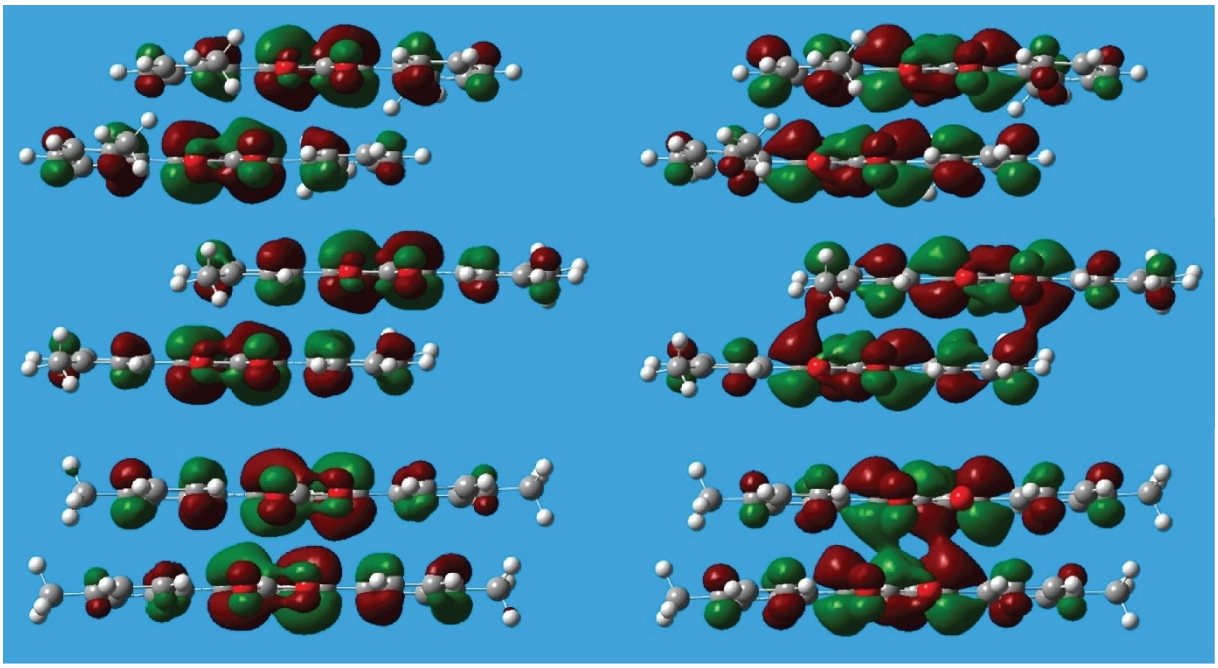

Figure 12. Highest occupied (H, left in a given pair) and lowest unoccupied (L, right) NTOs for the first forbidden transitions of **3 b** (dimer **3**, up), **3 c** (dimer **5**, middle) and **3 d** (dimer **1**, down) by TD DFT (ωB97X-D/6-31G(d,p)). Isovalue is always 0.022, the weights of a hole→particle (HNTO→LNTO) monoexcitation for a given transition are 65.0% (**3 b**), 74.2% (**3 c**) and 87.6% (**3 d**). Central dimers were extracted from π-stacked tetramers, optimized at M06-2X/6-311G(d,p) level.

Both π-isoelectronic compounds form the same π-stack in dimer 1 fashion with similar CCs and PPs[15,17a], but strongly differ in the tightness of in-layer binding, given by weak CH-HC contacts for **3 d** and four strong CO-HN hydrogen bonds per each molecule for DPP pigment. Although usually a restriction of excited state motion leads to stronger SSF of the monomers in solids, due to the restricted access to conical intersection,[10] in the case of P.R. 255 and other DPP pigments an opposite process, i.e. fixation restricted excimer formation and thus an absence of excimer-type SSF, may occur.

Conclusions

Diaryl substituted furofuranones are almost planar chromophores, π-isoelectronic with more famous diketopyrrolopyrroles, able to form the same set of centrosymmetrical slipped π-stacks in crystal columns, according to DFT based modelling. Four of these eight possible stack arrangements were found experimentally for phenyl derivative and three tolyl regioisomers, forming thus a support for previously reported theoretical concept, based on electron repulsion minimization principle. Both parent diphenyl derivatives of DFF and isoDFF form less stable π-stacks, fixed in crystals by other specific intermolecular interactions. Methyl substituents on phenyl limit or disable these supporting interactions and force DFF derivatives to adopt various, more stable, generally more compact and self-standing slipped π-stack crystal arrangements, specifically depending of methyl positions. Fluorescence of DFF derivatives in solution comes from rigid planar excited states, their spectral maxima lie within relatively sharp interval in blue/green region and depend solely on weak electronic effect of methyl substituent(s). There were found three types of photophysical behaviour, following light absorption of polycrystalline powders, depending exclusively on an arrangement of slipped stacks: never observed within DPPs J-type yellow emission for crystal with dimer **6** type closely π-stacked columns, common H-type quenching for dimer **3** moderately stacked arrangements and considerably bathochromically shifted orange to red H-type excimer fluorescence for dimers stacked in **1** and **5** fashion in crystal, specific by a CT character of the lowest lying state and weak fixing of the molecules in-layers. Furofuranones are thus versatile organic chromophores with solid-state optical properties gently tunable by simple structural changes.

Experimental section

Synthesis

All reagents and solvents were purchased from commercial sources (Sigma–Aldrich, Fluorochem, Acros Organics, TCI Europe, Merck, and Lach-Ner). Commercial grade reagents were used without further purification. Reactions were monitored by using thin-layer chromatography (TLC) plates coated with 0.2 mm silica gel (60 F254, Merck). TLC plates were visualized by using UV irradiation (254 nm). All melting points were determined by using a Melting Point B-540 apparatus (Büchi, Switzerland) and are given in their uncorrected form. The FTIR spectra were recorded with a FTIR Nicolet iS50 using the ATR technique. The NMR spectra were measured in $CDCl_3$ and C_6D_6-d_6 solutions at ambient temperature with a Bruker AscendTM 500 spectrometer at frequencies

500.13 MHz (^{1}H) and 125.76 MHz (^{13}C{^{1}H}). The chemical shifts (d) reported in text are given in ppm and are related to the following residual solvent peaks: @7.16 (C_6D_6-d_6), @7.27 ($CDCl_3$). Tetramethylsilane (TMS) was used as an internal standard. The coupling constants (*J*) are reported in Hz. Elemental analyses (C, H, and N) were performed with an automatic microanalyzer (Flash 2000 Organic elemental analyzer). Mass spectrometry with high resolution was determined by the "dried droplet" method using a MALDI mass spectrometer LTQ Orbitrap XL (Thermo Fisher Scientific) equipped with a nitrogen UV laser (337 nm, 60 Hz). Spectra were measured in positive ion mode and in regular mass extent with a resolution of 100000 at a mass-to-charge ratio (m/z) of 400, with 2,5-dihydrobenzoic acid (DBH) used as the matrix. All ethyl 3-oxo-3-phenylpropanoates **1 a–f** were synthesized according to the literature.[39]

General procedure A: Synthesis of diethyl 2,3-dibenzoylsuccinates (2 b–c)

The diethyl 2,3-dibenzoylsuccinates (**2 b–c**) were synthetized according to modified literature.[40] To a one-necked flask was added ethyl benzoyl acetate (1 mmol) which was dissolved in CH_3OH (2 mL) and CH_3CN (4 mL). Mixture was cooled to −20 °C and solution of Ammonium cerium(IV) nitrate (1.1 mmol, CAN) in H_2O (2 mL) was added dropwise during 5 minutes. Mixture turned to black and it was stirred at the same temperature for another 30 min (checked by TLC), and H_2O was added. The organic layer was separated, and the aqueous layer was extracted with EtOAc (3×10 mL). The combined organic phase was dried over Na_2SO_4, filtrated and evaporated. The crude oily product was crystallized from cold ethanol and EtOAc.

General procedure B: Synthesis of diethyl 2,3-dibenzoylsuccinates (2 a,d–f)

The Diethyl 2,3-dibenzoylsuccinates (**2 a,d–f**) were synthetized according to modified literature.[41] A flame-dried three-necked flask was charged dry Et_2O (3 mL) and fresh sliced sodium (1.01 mmol) under nitrogen atmosphere. To the heterogeneous mixture was slowly added solution of ethyl benzoyl acetate **1** (1 mmol) in dry Et_2O (1.3 mL). Then the mixture was allowed to stir at RT for 18 h. Next day was sodium completely consumed and the solution of iodine (1 mmol) in dry Et_2O (0.8 mL) was slowly added (60 min) with vigorous stirring. The brown mixture was allowed to stir at RT for 2 h and then the saturated solution of sodium thiosulfate was added. After separation of organic phase the water phase was extracted with EtOAc (3×10 mL), combined organic phases were dried over Na_2SO_4, filtrated and evaporated. The crude oily product was crystallized from cold ethanol and EtOAc.

Diethyl 2,3-dibenzoylsuccinate (2 a)

The title compound was prepared following general **procedure B**, using sodium (1 g, 43.5 mmol), commercial ethyl 3-oxo-3-phenylpropanoate (8.25 g, 42.9 mmol), iodine (5.54 g, 21.8 mmol) and dry Et_2O (200 mL). The crude product was crystallized from cold ethanol to provide the title compound (1.3 g, 16% yield) as a white crystals. **R_f**: 0.42 (*n*-hexan/EtOAc = 3/1, v/v), **m.p.**: 123–126 °C. **IR (ATR, cm^{-1})**: 2980, 1724, 1673, 1594,1577, 1448, 1366, 1285, 1247, 1203, 1180, 1019, 998, 852, 776, 740, 691, 634, 564. **^{1}H NMR**: (500 MHz, $CDCl_3$): δ = 8.22-8.17 (m, 2H, Ar-*H*), 7.67-7.61 (m, 1H, Ar-*H*), 7.57-7.51 (m, 1H, Ar-*H*), 5.64 (s, 1H, C*H*), 3.99 (q, *J* = 6.54 Hz, 2H, C*H*$_2$), 0.99 (t, *J* = 6.55 Hz, 3H, C*H*$_3$). **^{13}C NMR** (100 MHz, $CDCl_3$): δ = 194.0, 167.1, 136.2, 133.8, 129.4, 128.6, 62.1, 53.3, 13.6. **MALDI-TOF**: $[M+Na]^+$ Calcd. for $C_{22}H_{22}O_6$ 405.13086; found 405.13140. **Elemental analysis**: Calc. for $C_{22}H_{22}O_6$: C, 69.10; H, 5.80, found: C, 69.34 ± 0.03; H, 5.77 ± 0.01.

Diethyl 2,3-bis(2-methylbenzoyl)succinate (2 b)

The title compound was prepared following general **procedure A**, using CAN (45 g, 82.1 mmol), ethyl 3-oxo-3-(*o*-tolyl)propanoate (15 g, 72.7 mmol), CH_3OH (150 mL), CH_3CN (300 mL) and H_2O (150 mL). The crude product was crystallized from EtOH and EtOAc to provide the title compound (2 g, 13% yield) as a white crystals. **R_f**: 0.45 (*n*-hexan/EtOAc = 3/1, v/v), **m.p.**: 131–136 °C. **IR (ATR, cm^{-1})**: 2985, 1724, 1683, 1600, 1573, 1458, 1366, 1298, 1277, 1250, 1165, 1016, 994, 855, 767, 734, 633, 571, 498, 455. **^{1}H NMR**: (500 MHz, $CDCl_3$, mixture of epimers): δ = 8.13-8.05 (m, 2H, Ar-*H*), 7.47-7.26 (m, 6H, Ar-*H*), 5.48 (s, 1H, C*H*), 5.40 (s, 1H, C*H*), 4.04-3.98 (m, 4H, C*H*$_2$), 2.51 (s, 1H, C*H*), 2.45 (s, 1H, C*H*), 1.06-0.99 (m, 6H, C*H*$_3$). **^{13}C NMR**: (100 MHz, $CDCl_3$, mixture of epimers): δ = 197.7, 197.6, 168.1, 168.1, 139.7, 139.6, 132.7, 132.6, 32.4, 132.3, 130.5, 130.4, 126.5, 126.4, 62.7, 62.6, 56.96, 56.9, 21.7, 21.6, 14.4, 14.3. **MALDI-TOF**: $[M+Na]^+$ Calcd. for $C_{24}H_{26}O_6$ 433.16216; found 433.16279. **Elemental analysis**: Calc. for $C_{24}H_{26}O_6$: C, 70.23; H, 6.38, found: C, 70.61 ± 0.01; H, 6.26 ± 0.01.

Diethyl 2,3-bis(3-methylbenzoyl)succinate (2 c)

The title compound was prepared following general **procedure A**, using CAN (3 g, 5.5 mmol), ethyl 3-oxo-3-(*m*-tolyl)propanoate (1 g, 5 mmol), CH_3OH (10 mL), CH_3CN (20 mL) and H_2O (10 mL). The crude product was crystallized from EtOH and EtOAc to provide the title compound (0.2 g, 20% yield) as a white crystals. **R_f**: 0.45 (*n*-hexan/EtOAc = 3/1, v/v), **m.p.**: 105–108 °C. **IR (ATR, cm^{-1})**: 2983, 1728, 1673, 1600, 1446, 1366, 1288, 1255, 1217, 1148, 1022, 951, 858, 829, 789, 731, 688, 639, 564, 495, 465. **^{1}H NMR**: (500 MHz, $CDCl_3$): δ = 8.01–8.00 (m, 2H, Ar-*H*), 7.46–7.41 (m, 2H, Ar-*H*), 5.62 (s, 1H, C*H*), 3.98 (q, *J* = 7.12 Hz, 2H, C*H*$_2$), 2.47 (s, 3H, C*H*$_3$), 1.00 (t, *J* = 7.10 Hz, 2H, C*H*$_3$). **^{13}C NMR**: (100 MHz, $CDCl_3$): δ = 194.9, 167.9, 139.1, 136.9, 135.3, 130.6, 129.2, 127.4, 62.7, 54.0, 22.1, 14.4. **MALDI-TOF**: $[M+Na]^+$ Calcd. for $C_{24}H_{26}O_6$ 433.16216; found 433.16303. **Elemental analysis**: Calc. for $C_{24}H_{26}O_6$: C, 70.23; H, 6.38, found: C, 70.58 ± 0.03; H, 6.51 ± 0.05.

Diethyl 2,3-bis(4-methylbenzoyl)succinate (2 d)

The title compound was prepared following general **procedure B**, using sodium (1.46 g, 63.6 mmol), ethyl 3-oxo-3-(*p*-tolyl)propanoate (13 g, 63.03 mmol), iodine (16.15 g, 63.6 mmol) and dry Et_2O (250 mL). The crude product was crystallized from cold ethanol to provide the title compound (6 g, 46% yield) as a white crystals. **R_f**: 0.39 (*n*-hexan/EtOAc = 3/1, v/v), **m.p.**: 98–105 °C. **IR (ATR, cm^{-1})**: 2985, 1726, 1670, 1603, 1572, 1445, 1366, 1317, 1285, 1180, 1162, 1018, 855, 807, 704, 611, 579, 541, 473. **^{1}H NMR**: (500 MHz, $CDCl_3$, mixture of epimers): δ = 8.10 (d, 2H, *J* = 8.10 Hz, Ar-*H*), 8.03 (d, 2H, *J* = 8.73 Hz, Ar-*H*), 7.33 (d, 2H, *J* = 8.10 Hz, Ar-*H*), 7.29 (d, 2H, *J* = 8.73 Hz, Ar-*H*), 5.60 (s, 1H, C*H*), 5.54 (s, 1H, C*H*), 4.18–4.14 (m, 2H, C*H*$_2$), 4.00–4.96 (m, 2H, C*H*$_2$), 2.45 (s, 3H, C*H*$_3$), 2.43 (s, 3H, C*H*$_3$), 1.18 (t, *J* = 6.91 Hz, 3H, C*H*$_3$), 0.99 (t, *J* = 6.91 Hz, 3H, C*H*$_3$). **^{13}C NMR**: (100 MHz, $CDCl_3$): δ = 193.6, 192.6, 167.8, 167.3, 144.8, 144.7, 133.7, 133.3, 129.6, 129.5, 129.3, 129.2, 61.98, 61.94, 54.0, 53.2, 21.7, 13.8, 13.7. **MALDI-TOF**: $[M+Na]^+$ Calcd. for $C_{24}H_{26}O_6$ 433.16216; found 433.16325. **Elemental analysis**: Calc. for $C_{24}H_{26}O_6$: C, 70.23; H, 6.38, found: C, 70.58 ± 0.04; H, 6.47 ± 0.04.

Diethyl 2,3-bis(2,4-dimethylbenzoyl)succinate (2 e)

The title compound was prepared following general **procedure B**, using sodium (1.27 g, 55.2 mmol), ethyl 3-(2,4-dimethylphenyl)-3-oxopropanoate (12 g, 54.48 mmol), iodine (13.8 g, 54.5 mmol) and dry Et_2O (250 mL). The crude product was crystallized from cold ethanol to provide the title compound (2.22 g, 18% yield) as a white crystals. **R_f**: 0.49 (*n*-hexan/EtOAc = 3/1, v/v), **m.p.**: 114–118 °C. **IR (ATR, cm^{-1})**: 2985, 2918, 1716, 1672, 1610, 1564, 1444, 1365, 1277, 1251, 1150, 1093, 1021, 990, 854, 811, 796, 774, 747, 628, 581, 540, 434. **^{1}H NMR**: (500 MHz, $CDCl_3$, mixture of epimers and diethyl 2,3-bis(2,4-dimethylbenzoyl)fumarate): δ = 8.02 (d, 2H, *J* = 8.21 Hz, Ar-*H*), 7.68 (d, 2H, *J* = 7.12 Hz, Ar-*H*), 7.17-7.09 (m, 6H, Ar-*H*), 5.42 (s, 2H, 2xC*H*), 4.06-3.96 (m, 6H, CH_2), 2.70 (s, 3H, CH_3), 2.47 (s, 6H, CH_3), 2.39 (s, 9H, CH_3), 1.04-0.98 (m, 9H, CH_3). **^{13}C NMR**: (100 MHz, $CDCl_3$): δ = 196.3, 192.2, 167.6, 163.2, 143.6, 142.7, 142.2, 140.7, 139.5, 139.0, 134.1, 133.1, 132.7, 132.0, 131.9, 130.4, 126.5, 126.4, 62.4, 61.8, 55.9, 21.8, 21.6, 21.5, 21.3, 21.2, 13.7, 13.5. **MALDI-TOF**: $[M+Na]^+$ Calcd. for $C_{26}H_{30}O_6$ 461.19346; found 461.19459. **Elemental analysis**: Calc. for $C_{26}H_{30}O_6$: C, 71.21; H, 6.90, found: C, 71.03 ± 0.06; H, 6.91 ± 0.02.

Diethyl 2,3-bis(3,5-dimethylbenzoyl)succinate (2 f)

The title compound was prepared following general **procedure B**, using sodium (1.17 g, 51 mmol), ethyl 3-(3,5-dimethylphenyl)-3-oxopropanoate (11 g, 54.48 mmol), iodine (12.7 g, 50 mmol) and dry Et_2O (250 mL). The crude product was crystallized from cold ethanol to provide the title compound (6.6 g, 60% yield) as a white crystals. **R_f**: 0.5 (*n*-hexan/EtOAc = 3/1, v/v), **m.p.**: 126–129 °C. **IR (ATR, cm^{-1})**: 2984, 2916, 1735, 1682, 1596, 1445, 1366, 1302, 1282, 1263, 1246, 1207, 1183, 1158, 1139, 1096, 1024, 889, 858, 821, 682, 633, 553, 450, 415. **^{1}H NMR**: (500 MHz, $CDCl_3$, mixture of epimers): δ = 7.81-7.69 (m, 4H, Ar-*H*), 7.28-7.20 (m, 2H, Ar-*H*), 5.59 (s, 1H, C*H*), 5.52 (s, 1H, C*H*), 4.19-4.14 (m, 2H, CH_2), 4.02-4.94 (m, 2H, CH_2), 2.43 (s, 3H, CH_3), 2.39 (s, 3H, CH_3), 2.34 (s, 3H, CH_3), 2.32 (s, 3H, CH_3), 1.21-1.14 (m, 3H, CH_3), 1.04-0.96 (m, 3H, CH_3). **^{13}C NMR**: (100 MHz, $CDCl_3$, mixture of epimers): δ = 195.1, 164.1, 168.5, 168.0, 138.9, 138.8, 136.96, 136.9, 136.54, 136.5, 136.2, 136.1, 127.9, 127.8, 62.7, 62.6, 54.9, 54.0, 21.9, 14.6, 14.3. **MALDI-TOF**: $[M+Na]^+$ Calcd. for $C_{26}H_{30}O_6$ 461.19346; found 461.19447. **Elemental analysis**: Calc. for $C_{26}H_{30}O_6$: C, 71.21; H, 6.90, found: C, 71.57 ± 0.14; H, 7.02 ± 0.09.

General procedure for synthesis of 3,6-diphenyl-1H,4H-furo[3,4-c]furan-1,4-dione (DFFs 3 a–f)

The 3,6-diphenyl-1*H*,4*H*-furo[3,4-*c*]furan-1,4-diones were synthetized according to modified literature.[33] A three-necked flask was charged with diethyl 2.3-bis(2-methylbenzoyl)succinates which were slowly heated in vacuo (1 mbar/250 °C), cooled down (220–230 °C) and heated up again. After a further cooling-heating cycle the was mixture cooled down and EtOAc were added (target material is very slightly soluble in EtOAc). Crude DFFs were filtrated washed with EtOAc and dried.

3,6-diphenyl-1H,4H-furo[3,4-c]furan-1,4-dione (3 a)

The title compound was prepared following general procedure, using diethyl 2,3-dibenzoylsuccinate (0.5 g, 1.3 mmol) The crude product was rinsed with EtOAc to provide the title compound (0.12 g, 32% yield) as an orange crystals. **R_f**: 0.5 (*n*-hexan/EtOAc = 3/1, v/v), **m.p.**: > 300 °C. **IR (ATR, cm^{-1})**: 1774, 1739, 1626, 1569, 1490, 1448, 1303, 1115, 1058, 953, 810, 771, 746, 713, 684, 633, 443, 421. **^{1}H NMR**: (500 MHz, C_6D_6): δ = 8.17-8.15 (d, 2H, *J* = *7.58 Hz*, Ar-*H*), 7.05-6.98 (m, 3H, Ar-*H*). **^{13}C NMR**: (100 MHz, C_6D_6): δ = 158.6, 156.4, 156.4, 133.6, 129.7, 128.7, 127.2, 110.2. **MALDI-TOF**: $[M+H]^+$ Calcd. for $C_{18}H_{10}O_4$ 291.06519; found 291.06558. **Elemental analysis**: Calc. for $C_{20}H_{14}O_4$: C, 74.48; H, 3.47, found: C, 74.18 ± 0.03; H, 3.41 ± 0.01.

3,6-di-*o*–tolyl-1*H*,4*H*-furo[3,4-*c*]furan-1,4-dione (3 b)

The title compound was prepared following general procedure, using diethyl 2,3-bis(2-methylbenzoyl)succinate (2 g, 4.87 mmol) The crude product was rinsed with EtOAc to provide the title compound (0.15 g, 10% yield) as an orange crystals. **R_f**: 0.53 (*n*-hexan/EtOAc = 3/1, v/v), **m.p.**: 234.5–236.8 °C. **IR (ATR, cm^{-1})**: 1773, 1752, 1591, 1559, 1438, 1381, 1328, 1282, 1203, 1170, 1134, 1108, 1044, 947, 834, 768, 723, 648, 485, 460, 436. **^{1}H NMR**: (500 MHz, C_6D_6): δ = 8.53 (d, 1H, *J* = 8.78 Hz, Ar-*H*), 7.03 (t, 1H, *J* = 7.53 Hz, Ar-*H*), 6.96 (t, 1H, *J* = 7.53 Hz, Ar-*H*), 6.83 (d, 1H, *J* = 7.53 Hz, Ar-*H*), 2.48 (s, 3H, CH_3). **^{13}C NMR**: (100 MHz, C_6D_6): δ = 158.9, 158.6, 139.5, 133.3, 132.9, 131.8, 128.7, 127.1, 126.3, 110.2, 22.7. **MALDI-TOF**: $[M+H]^+$ Calcd. for $C_{20}H_{14}O_4$ 319.09649; found 319.09677. **Elemental analysis**: Calc. for $C_{20}H_{14}O_4$: C, 75.46; H, 4.43, found: C, 75.45 ± 0.03; H, 4.27 ± 0.01.

3,6-di-*m*-tolyl-1*H*,4*H*-furo[3,4-*c*]furan-1,4-dione (3 c)

The title compound was prepared following general procedure, using diethyl 2,3-bis(3-methylbenzoyl)succinate (2.5 g, 6.09 mmol) The crude product was rinsed with EtOAc to provide the title compound (0.59 g, 31% yield) as an red crystals. **R_f**: 0.55 (*n*-hexan/EtOAc = 3/1, v/v), **m.p.**: > 300 °C. **IR (ATR, cm^{-1})**: 1771, 1714, 1631, 1595, 1579, 1486, 1331, 1204, 1073, 963, 887, 790, 746, 722, 688, 491, 437, 424. **^{1}H NMR**: (500 MHz, C_6D_6): δ = 8.12 (d, 1H, *J* = 7.45 Hz, Ar-*H*), 8.03 (s, 1H, Ar-*H*), 7.02 (t, 1H, *J* = 7.45 Hz, Ar-*H*), 6.87 (d, 1H, *J* = 7.45 Hz, Ar-*H*), 2.03 (s, 3H, CH_3). **^{13}C NMR**: (100 MHz, C_6D_6): 158.02, 155.9, 138.9, 133.9, 129.0, 128.3, 126.6, 125.5, 109.4, 20.7. **MALDI-TOF**: $[M+H]^+$ Calcd. for $C_{20}H_{14}O_4$ 319.09649; found 319.09685. **Elemental analysis**: Calc. for $C_{20}H_{14}O_4$: C, 75.46; H, 4.43, found: C, 74.87 ± 0.02; H, 4.32 ± 0.01.

3,6-di-*p*–tolyl-1*H*,4*H*-furo[3,4-*c*]furan-1,4-dione (3 d)

The title compound was prepared following general procedure, using diethyl 2,3-bis(4-methylbenzoyl)succinate (0.65 g, 1.58 mmol) The crude product was rinsed with EtOAc to provide the title compound (0.22 g, 44% yield) as an red crystals. **R_f**: 0.54 (*n*-hexan/EtOAc = 3/1, v/v), **m.p.**: > 300 °C. **IR (ATR, cm^{-1})**: 1778, 1629, 1562, 1505, 1413, 1324, 1178, 1093, 1054, 944, 815, 745, 722, 636, 470. **^{1}H NMR**: (500 MHz, C_6D_6): δ = 8.15 (d, 2H, *J* = 8.01 Hz, Ar-*H*), 6.87 (d, 2H, *J* = 8.01 Hz, Ar-*H*), 1.92 (s, 3H, CH_3). **^{13}C NMR**: (100 MHz, C_6D_6): 158.2, 155.6, 129.8, 128.0, 124.1, 108.8, 21.3. **MALDI-TOF**: $[M+H]^+$ Calcd. for $C_{20}H_{14}O_4$ 319.09649; found 319.09693. **Elemental analysis**: Calc. for $C_{20}H_{14}O_4$: C, 75.46; H, 4.43, found: C, 75.90 ± 0.02; H, 4.32 ± 0.05.

3,6-bis(2,4-dimethylphenyl)-1*H*,4*H*-furo[3,4-*c*]furan-1,4-dione (3 e)

The title compound was prepared following general procedure, using Diethyl 2,3-bis(2,4-dimethylbenzoyl)succinate (0.5 g, 1.14 mmol) The crude product was rinsed with EtOAc to provide the title compound (0.2 g, 51% yield) as an red crystals. **R_f**: 0.53 (*n*-hexan/EtOAc = 3/1, v/v), **m.p.**: > 300 °C. **IR (ATR, cm^{-1})**: 1770, 1733, 1598, 1437, 1383, 1325, 1232, 1232, 1190, 1142, 1101, 1040, 951, 821, 734, 712, 640, 596, 529, 475, 442. **^{1}H NMR**: (500 MHz, C_6D_6): δ = 8.54 (d, 1H, *J* = 7.37 Hz, Ar-*H*), 6.86 (d, 1H, *J* = 8.54 Hz, Ar-*H*), 6.69 (s, 1H, Ar-*H*), 2.51 (s, 3H, CH_3), 1.94 (s, 3H, CH_3). **^{13}C NMR**: (100 MHz, C_6D_6): 158.9, 158.8, 144.1, 139.4, 133.8, 132.0, 128.7, 128.0, 123.9,

22.7, 21.8. **MALDI-TOF**: $[M+H]^+$ Calcd. for $C_{22}H_{18}O_4$ 347.12779; found 347.12828. **Elemental analysis**: Calc. for $C_{22}H_{18}O_4$: C, 76.29; H, 5.24, found: C, 76.57 ± 0.07; H, 5.32 ± 0.02.

3,6-bis(3,5-dimethylphenyl)-1*H*,4*H*-furo[3,4-*c*]furan-1,4-dione (3 f)

The title compound was prepared following general procedure, using Diethyl 2,3-bis(2,4-dimethylbenzoyl)succinate (0.5 g, 1.14 mmol) The crude product was rinsed with EtOAc to provide the title compound (0.12 g, 32% yield) as an orange crystals. **R_f**: 0.58 (*n*-hexan/EtOAc = 3/1, v/v), **m.p.**: > 300 °C. **IR (ATR, cm^{-1})**: 1769, 1723, 1633, 1590, 1435, 1378, 1334, 1229, 1116, 1080, 1042, 958, 943, 889, 863, 750, 726, 692, 651, 544, 517, 487. **^{1}H NMR**: Due to the abnormal insolubility in most commonly used NMR solvents, it was impossible to measure the appropriate spectra of compound **3 f**. **MALDI-TOF**: $[M+H]^+$ Calcd. for $C_{22}H_{18}O_4$ 347.12779; found 347.12832. **Elemental analysis**: Calc. for $C_{22}H_{18}O_4$: C, 76.29; H, 5.24, found: C, 76.63 ± 0.01; H, 5.18 ± 0.06.

X-Ray Single Crystal Analysis

Single-crystal X-ray diffraction data of **3 a, 3 c–3 e** were collected at 150 K on an Agilent Technologies SuperNova Dual diffractometer with an Atlas detector using Mo–Kα ($\lambda = 0.71073$ Å) or Cu–Kα radiation ($\lambda = 1.54184$ Å). The data were processed using CrysAlis Pro[41]. Structures were solved by SHELXT [42] using intrinsic phasing and refined by a full-matrix least-squares procedure based on F^2 with SHELXL[43] using Olex2 program suite[44]. All the non-hydrogen atoms were refined anisotropically. Hydrogen atoms were readily located in difference Fourier maps, and were subsequently treated as riding atoms in geometrically idealized positions. In the crystal structure of **3 d** the furofuranone scaffold was refined as disordered over two positions in 0.522(3):0.478(3) ratio. Furthermore, C and O atoms of furofuranone scaffold were refined restraining the bonding distances as well as restrained to have similar U_{ij} components.

The crystallographic data are listed in Table S1. Deposition Numbers 2260329 (for **4 a**), 2260330 (for **4 c**), 2260331 (for **4 d**), 2260332 (for **4 e**) contain the supplementary crystallographic data for this paper. These data are provided free of charge by the joint Cambridge Crystallographic Data Centre and Fachinformationszentrum Karlsruhe Access Structures service.

Absorption and Fluorescence

The absorption spectra were measured on a Hewlett Packard 8453 UV/vis spectrophotometer. The stock solutions were prepared by dissolving ca 1 mg of sample in 25 mL DCM and then diluted 1 : 10. To measure fluorescence quantum yields, the solutions with optical density ≤ 0.05 at absorption maximum in 1-cm cell were prepared immediately before use. The steady-state fluorescence spectra were measured using a PTI Quanta Master 30 spectrophotometer. The instrument provides corrected excitation spectra directly; the fluorescence emission spectra were corrected for the characteristics of the emission monochromator and for the detection of photomultiplier response. During fluorescence measurements, weakly absorbing solutions (optical density less than ca 0.05 at the exciting wavelengths in 1-cm cell) were used. The fluorescence quantum yields (q_{Fl}) were measured using quinine sulphate (fluorescence quantum yield $q_{Fl} = 0.54$ in 0.5 mol/L H_2SO_4) [45, 46] as the standard. Deoxygenation of the samples by bubbling through N_2 did not make any difference in the spectra and/or quantum yields evaluated; therefore, the data reported here correspond to aerated solutions. DCM used was of spectral grade and was checked for its own fluorescence under relevant conditions. Solid state fluorescence was measured using powdered samples.

Quantum chemical calculations

Final geometries of centrosymmetrical either cofacial slipped stacked dimers and tetramers or 3x2 hexamers with three CO-HC bonded molecules in each of two stacked layers, bonded either in 23 or 34 fashion (Figure S1), were obtained using DFT with M06-2X[47] xc functional by full geometrical optimization, starting from various centrosymmetrical geometries. No symmetrical constraints were used. The geometries were computed first with 6-31G(d,p) basis set and checked by vibrational analysis, and then recomputed with 6-311G(d,p) basis set. Binding energies of the central dimers extracted from the optimized 3x2 hexamers were computed as the difference between dimer energy, obtained with the same functionals using an extended 6-311 + G(2d,p) basis sets with involved counterpoise (CP) procedure,[48], and optimized monomer energy, obtained in a same way. Zero-point energy corrections were not evaluated. All calculations were carried out with Gaussian 09 software.[49] The resulting geometries were characterized by plane-to-plane (PP) and centre-to-centre (CC) distances between DFF cores of both monomers in a dimer.[15] Computed PP and CC were evaluated by Mercury 3.9.[50] Excitation energies of the lowest six singlet states of the dimers were computed by TD DFT with ωB97X-D[51] xc functional and 6-311 + G(2d,p) basis set. Monomers in DCM were studied by an optimization of a geometry in the ground (DFT) and the lowest excited (TD DFT) state using CAM-B3LYP[52] xc functional, 6-311G(d,p) basis set and a solvent effect introduced by polarized continuum model (PCM).

Acknowledgements

The authors thank for their financial support the Czech Science Foundation grant No. 19-22783S. Computational resources were supplied by the project "e-Infrastruktura CZ" (e-INFRA CZ LM2018140) supported by the Ministry of Education, Youth and Sports of the Czech Republic. F. P. thanks Slovenian Research Agency (P1-0230-0175) for financial support and EN–FIST Centre of Excellence, Slovenia, for the use of the Supernova diffractometer. The authors also wish to thank Maksim Andreevich Samsonov, Ph.D. (Dept. of General and Inorganic Chemistry, University of Pardubice) for his help in solving the "twinned structure" of the single crystal of substance 3d.

Conflict of Interests

The authors declare no conflict of interest.

Data Availability Statement

The data that support the findings of this study are available from the corresponding author upon reasonable request.

Keywords: fluorescence · density functional theory · furofuranones · diketopyrrolopyrroles · polymorphism · regioisomerism

[1] a) H. Sirringhaus, *Adv. Mater.* **2014**, *26*, 1319–1335; b) H. Dong, X. Fu, J. Liu, Z. Wang, W. Hu, *Adv. Mater.* **2013**, *25*, 6158–6183; c) Y. Zhao, Y. Guo, Y. Liu, *Adv. Mater.* **2013**, *25*, 5372–5391.
[2] a) C. Wang, H. Dong, L. Jiang, W. Hu, *Chem. Soc. Rev.* **2018**, *47*, 422–500; b) G. Grynova, K. H. Lin, C. Corminboeuf, *J. Am. Chem. Soc.* **2018**, *140*, 16370–16386.
[3] Z. Zhang, L. Jiang, C. Cheng, Y. Zhen, G. Zhao, H. Geng, Y. Yi, L. Li, H. Dong, Z. Shuai, W. Hu, *Angew. Chem. Int. Ed.* **2016**, *55*, 5206–5209.
[4] a) G. Schweicher, V. Lemaur, C. Niebel, C. Ruzié, Y, Diao, O. Goto, W. Lee, Y. Kim, J.-B. Arlin, J. Karpinska, A. R. Kennedy, S. R. Parkin, Y. Olivier, S. C. B. Mannsfeld, J. Cornil, Y. H. Geerts, Z. Bao, *Adv. Mater.* **2015**, *27*, 3066–3072; b) Y. Tsutsui, G. Schweicher, B. Chattopadhyay, T. Sakurai, J.-B. Arlin, C. Ruzié, A. Aliev, A. Ciesielski, S. Colella, A. R. Kennedy, V. Lemaur, Y. Olivier, R. Hadji, L. Sanguinet, F. Castet, S. Osella, D. Dudenko, D. Beljonne, J. Cornil, P. Samori, S. Seki, Y. H. Geerts, *Adv. Mater.* **2016**, *28*, 7106–7114; c) S. Inoue, T. Higashino, S. Arai, R. Kumai, H, Matsui, S. Tsuzuki, S. Horiuchi, T. Hasegawa, *Chem. Sci.* **2020**, *11*, 12493–12505.
[5] a) F. C. Spano, *Acc. Chem. Res.* **2010**, *43*, 429–439; b) N. J. Hestand, F. C. Spano, *Acc. Chem. Res.* **2017**, *50*, 341–350; c) N. J. Hestand, F. C. Spano, *Chem. Rev.* **2018**, *118*, 7069–7163.
[6] a) M. Liu, Y. Wei, Q. Ou, P. Yu, G. Wang, Y. Duan, H. Geng, Q. Peng, Z. Shuai, Y. Liao, *J. Phys. Chem. Lett.* **2021**, *12*, 938–946; b) Q. Sun, J. Ren, T. Yiang, Q. Peng, Q. Ou, Z. Shuai, *Nano Lett.* **2021**, *21*, 5394–5400; c) Q. Sun, T. Jiang, Q. Ou, Q. Peng, Z. Shuai, *Adv. Opt. Mater.* **2022**, *10*, 2202262.
[7] a) Z. Qin, H. Gao, H. Dong, W. Hu, *Adv. Mater.* **2021**, *33*, 2007149; b) Z. Qin, H. Gao, H. Dong, W. Hu, *Adv. Opt. Mater.* **2022**, *10*, 2201644.
[8] Z. Qin, C. Gao, H. Gao, T. Wang, H. Dong, W. Hu, *Sci. Adv.* **2022**, *8*, eabp8775.
[9] a) J. L. Belmonte-Vázquez, Y. A. Amador-Sánchez, L. A. Rodríguez-Cortés, B. Rodriguez-Molina, *Chem. Mater.* **2021**, *33*, 7160–7184; b) A. Huber, J. Dubbert, T. D. Scherz, J. Voskuhl, *Chem. Eur. J.* **2023**, *29*, e202202481.
[10] J. Gierschner, J. Shi, B. Milián-Medina, D. Roca-Sanjuán, S. Varghese, S. Y. Park, *Adv. Opt. Mater.* **2021**, *9*, 2002251.
[11] J. Zhou, W. Zhang, X.-F. Jiang, C. Wang, X. Zhou, B. Xu, L. Liu, Z. Xie, Y. Ma, *J. Phys. Chem. Lett.* **2018**, *9*, 596–600.
[12] a) Q. Luo, L. Li, H. Ma, C. Lv, X. Jiang, X. Gu, Z, An, B. Zou, C. Zhang, Y. Zhang, *Chem. Sci.* **2020**, *11*, 6020–6025; b) Z. Sun, Q. Zang, Q, Luo, C. Lv, F. Cao, Q. Song, R. Zhao, Y. Zhang, W. Y. Wong, *Chem. Commun.* **2019**, *55*, 4735–4738; c) C. Lv, W. Liu, Q. Luo, H. Yi, H. Yu, Z. Yang, B. Zou, Y. Zhang, *Chem. Sci.* **2020**, *11*, 4007–4015.
[13] a) K. Pauk, S. Luňák Jr., A. Růžička, A. Marková, A. Mausová, M. Kratochvíl, K. Melánová, M. Weiter, A. Imramovský, M. Vala, *Chem. Eur. J.* **2021**, *27*, 4341–4348; b) K. Pauk, S. Luňák Jr., A. Růžička, A. Marková, K. Teichmanová, A. Mausová, M. Kratochvíl, R. Smolka, T. Mikysek, M. Weiter, A. Imramovský, M. Vala, *RSC Adv.* **2022**, *12*, 34797–34807.
[14] J. H. Kim, T. Schembri, D. Bialas, M. Stolte, F. Würthner, *Adv. Mater.* **2022**, *34*, 2104678.
[15] S. Luňák Jr., M. Weiter, M. Vala, *ChemPhysChem* **2022**, *23*, e202200252.
[16] a) A. Iqbal, M. Jost, R. Kirchmayer, J. Pfenninger, A. C. Rochat, O. Wallquist, *Bull. Soc. Chim. Belg.* **1988**, *97*, 615–643; b) Z. Hao, A. Iqbal, *Chem. Soc. Rev.* **1997**, *26*, 203–213.
[17] a) J. Mizuguchi, A. Grubenmann, G. Wooden, G. Rihs, *Acta Cryst. B48* **1992**, 696–700; b) J. Mizuguchi, A. Grubenmann, G. Rihs, *Acta Cryst. B49* **1993**, 1056–1060.
[18] a) M. Vala, J. Vyňuchal, P. Toman, M. Weiter, S. Luňák Jr., *Dyes Pigm.* **2010**, *84*, 176–182; b) S. Luňák Jr., L. Havel, J. Vyňuchal, P. Horáková, J. Kučerík, M. Weiter, R. Hrdina, *Dyes Pigm.* **2010**, *85*, 27–36.
[19] P. E. Hartnett, E. A. Margulies, C. M. Mauck, C. E. Miller, Y. Wu, Y. L. Wu, T. J. Marks, M. R. Wasielewski, *J. Phys. Chem. B* **2016**, *120*, 1357–1366.
[20] a) H. Langhals, T. Potrawa, H. Nöth, G. Linti, *Angew. Chem. Int. Ed.* **1989**, *28*, 478–480; b) S. Luňák Jr., J. Vyňuchal, M. Vala, L. Havel, R. Hrdina, *Dyes Pigm.* **2009**, *82*, 102–108; c) S. Luňák Jr., M. Vala, J. Vyňuchal, I. Ouzzane, P. Horáková, P. Možíšková, Z. Eliáš, M. Weiter, *Dyes Pigm.* **2011**, *91*, 269–278.
[21] a) J. Kuwabara, T. Yamagata, T. Kanbara, *Tetrahedron* **2010**, *66*, 3736–3741; b) S. Ghosh, D. S. Phillips, A. Saeki, A. Ajayaghosh, *Adv. Mater.* **2017**, *29*, 1605408; c) Z. Liu, K. Zhang, Q. Sun, Z. Zhang, L. Tang, S. Xue, D. Chen, H. Zhang, W. Yang, *J. Mater. Chem. C* **2018**, *6*, 1377–1383; d) A. Leventis, J. Royakkers, A. G. Rapidis, N. Goodeal, M. R. Corpinot, J. M. Frost, D. K. Bučar, M. O. Blunt, F. Cacialli, H. Bronstein, *J. Am. Chem. Soc.* **2018**, *140*, 1622–1626; e) T. G. Hwang, J. Y. Kim, J. W. Namgoong, J. M. Lee, S. B. Yuk, S. H. Kim, J. P. Kim, *Photochem. Photobiol. Sci.* **2019**, *18*, 1064–1074; f) Q. Yang, X. Sun, J. Han, L. Wang, *Dyes Pigm.* **2021**, *194*, 109655; g) Q. Yang, J. Zhang, L. Wang, *Dyes Pigm.* **2022**, *198*, 110024.
[22] a) E. D. Glowacki, H. Coskun, M. A. Blood-Forsythe, U. Monkowius, L. Leonat, M. Grzybowski, D. Gryko, M. S. White, A. Aspuru-Guzik, N. S. Sariciftci, *Org. Electron.* **2014**, *15*, 3521–3528; b) M. Kratochvíl, M. Ciganek, Ci. Yumusak, H. Seelajaroen, I. Cisařová, J. Fábry, M. Vala, S. Luňák, M. Weiter, N. S. Sariciftci, J. Krajcovic, *Dyes Pigm.* **2022**, *197*, 109884.
[23] a) S.L Suraru, U. Zschieschang, H. Klauk, F. Würthner, *Chem. Commun.* **2011**, *47*, 1767–1769; b) M. Stolte, S.L Suraru, P. Diemer, T. He, Ch. Burschka, U. Zschieschang, H. Klauk, F. Würthner, *Adv. Funct. Mater.* **2016**, *26*, 7415–7422; c) A. Kovalenko, C. Yumusak, P. Heinrichová, S. Stříteský, L. Fekete, M. Vala, M. Weiter, N. S. Sariciftci, J. Krajcovič, *J. Mater. Chem. C* **2017**, *5*, 4716–4723.
[24] a) B. Walker, A. B. Tamayo, X. D. Dang, P. Zalar, J. H. Seo, A. Garcia, M. Tantiwiwat, T. Q. Nguyen, *Adv. Funct. Mater.* **2009**, *19*, 3063–3069; b) P. Heinrichová, J. Pospíšil, S. Stříteský, M. Vala, M. Weiter, P. Toman, D. Rais, J. Pfleger, M. Vondráček, D. Šimek, L. Fekete, P. Horáková, L. Dokládalová, L. Kubáč, I. Kratochvílová, *J. Phys. Chem. C* **2019**, *123*, 11447–11463.
[25] S. Luňák Jr., J. Vyňuchal, R. Hrdina, *J. Mol. Struct.* **2009**, *919*, 239–245.
[26] M. Grzybowski, D. T. Gryko, *Adv. Opt. Mater.* **2015**, *3*, 280–320.
[27] R. F. Fernandes, A. B. Porto, L. S. Flores, L. F. Mai, C. C. Corrêa, A. S. Spielmann, H. G. M. Edwards, L. F. C. de Oliveira, *Vib. Spectrosc.* **2018**, *99*, 59–66.
[28] K. Kawabata, I. Osaka, M. Sawamoto, J. L. Zafra, P. M. Burrezo, J. Casado, K. Takimiya, *Chem. Eur. J.* **2017**, *23*, 4579–4589.
[29] T. Nagaoka, Y. Matsui, M. Fuki, T. Ogaki, E. Ohta, Y. Kobori, H. Ikeda, *ACS Omega* **2022**, *7, 40364–40373*.
[30] G. M. Fischer, A. P. Ehlers, A. Zumbusch, E. Daltrozzo, *Angew. Chem. Int. Ed.* **2007**, *46*, 3750–3753.
[31] T. Marks, E. Daltrozzo, A. Zumbusch, *Chem. Eur. J.* **2014**, *20*, 6494–6504.
[32] M. B. Rubin, M. Bargurie, S. Kosti, M. J. Kaftory, *J. Chem. Soc. Perkin Trans. 1* **1980**, 2670–2677.
[33] H. Langhals, T. Grundei, T. Potrawa, K. Polborn, *Liebigs Ann.* **1996**, 679–682.
[34] T. Lu, Y. T. Jiang, F. P. Ma, Z. J. Tang, L. Kuang, Y. X. Wang, B. Wang, *Org. Lett.* **2017**, *19*, 6344–6347.
[35] J. Song, H. Zhang, X. Chen, X. Li, D. Xu, *Synt. Comm.* **2010**, *40*, 1847–1855.
[36] K. Zhang, B. Tieke, *Macromolecules.* **2008**, *41*, 7287–7295.
[37] C. Zheng, C. Zhong, C. J. Collison, F. C. Spano, *J. Phys. Chem. C* **2019**, *123*, 3203–3215.
[38] T. Nematiaram, D. Padula, A. Troisi, *Chem. Mater.* **2021**, *33*, 3368–3378.
[39] A. P. Bialas, F. C. Spano, *J. Phys. Chem. C* **2022**, *126*, 4067–4081.
[40] M. Deutsch, S. Wirsing, D. Kaiser, R. F. Fink, P. Tegeder, B. Engels, *J. Chem. Phys.* **2020**, *153*, 224104.
[41] *CrysAlisPro*, version 1.171.39.46e; Rigaku Oxford Diffraction: Yarnton, UK, 2018.
[42] G. M. Sheldrick, *Acta Crystallogr.* **2015**, *A71*, 3–8.
[43] G. M. Sheldrick, *Acta Crystallogr.* **2015**, *C71*, 3–8.
[44] O. V. Dolomanov, L. J. Bourhis, R. J. Gildea, J. A. K. Howard, H. Puschmann, *J. Appl. Crystallogr.* **2009**, *42*, 339–341.
[45] J. B. Birks, D. J. Dyson, *Proc. R. Soc.* **1963**, *A275*, 135.
[46] W. R. Ware, B. A. Baldwin, *J. Chem. Phys.* **1964**, *40*, 1703.
[47] Y. Zhao, D. G. Truhlar, *Theor. Chem. Acc.* **2008**, *120*, 215–241.
[48] S. F. Boys, F. Bernardi, *Mol. Phys.* **2002**, *100*, 65–73.
[49] Gaussian 09, Revision **D.01**, M. J. Frisch, W. G. Trucks, H. B. Schlegel, G. E. Scuseria, M. A. Robb, J. R. Cheeseman, G. Scalmani, V. Barone, B. G. Mennucci, A. Petersson, H. Nakatsuji, M. Caricato, X. Li, H. P. Hratchian, A. F. Izmaylov, J. Bloino, G. Zheng, J. L. Sonnenberg, M. Hada, M. Ehara, K. Toyota, R. Fukuda, J. Hasegawa, M. Ishida, T. Nakajima, Y. Honda, O. Kitao, H. Nakai, T. Vreven, J. A. Montgomery Jr., J. E. Peralta, F. Ogliaro, M. Bearpark, J. J. Heyd, E. Brothers, K. N. Kudin, V. N. Staroverov, R. Kobayashi, J. Normand, K. Raghavachari, A.

Rendell, J. C. Burant, S. S. Iyengar, J. Tomasi, M. Cossi, N. Rega, J. M. Millam, M. Klene, J. E. Knox, J. B. Cross, V. Bakken, C. Adamo, J. Jaramillo, R. Gomperts, R. E. Stratmann, O. Yazyev, A. J. Austin, R. Cammi, C. Pomelli, J. W. Ochterski, R. L. Martin, K. Morokuma, V. G. Zakrzewski, G. A. Voth, P. Salvador, J. J. Dannenberg, S. Dapprich, A. D. Daniels, Ö. Farkas, J. B. Foresman, J. V. Ortiz, J. Cioslowski, D. J. Fox. C. T. Wallingford, Gaussian, Inc. 2009.

[50] C. F. Macrae, P. R. Edgington, P. McCabe, E. Pidcock, G. P. Shields, R. Taylor, M. Towler, J. van de Streek, *J. Appl. Crystallogr.* **2006**, *39*, 453–457.

[51] J. D. Chai, M. Head-Gordon, *Phys. Chem. Chem. Phys.* **2008**, *10*, 6615–6620.

[52] T. Yanai, D. P. Tew, N. C. Handy, *Chem. Phys. Lett.* **2004**, *393*, 51–57.

Manuscript received: June 29, 2023
Revised manuscript received: July 11, 2023
Accepted manuscript online: July 21, 2023
Version of record online: August 8, 2023